batteries

MDPI

Review

Understanding High-Voltage Behavior of Sodium-Ion Battery Cathode Materials Using Synchrotron X-ray and Neutron Techniques: A Review

Vadim Shipitsyn [1,2,†], Rishivandhiga Jayakumar [1,2,†], Wenhua Zuo [3,†], Bing Sun [4,*] and Lin Ma [1,2,*]

1 Department of Mechanical Engineering and Engineering Science, The University of North Carolina at Charlotte, Charlotte, NC 28223, USA; vshipits@charlotte.edu (V.S.); rjayakum@charlotte.edu (R.J.)
2 Battery Complexity, Autonomous Vehicle and Electrification (BATT CAVE) Research Center, The University of North Carolina at Charlotte, Charlotte, NC 28223, USA
3 Chemical Sciences and Engineering Division, Argonne National Laboratory, Lemont, IL 60439, USA; wzuo@anl.gov
4 Centre for Clean Energy Technology, School of Mathematical and Physical Sciences, Faculty of Science, University of Technology Sydney, Ultimo, NSW 2007, Australia
* Correspondence: bing.sun@uts.edu.au (B.S.); l.ma@charlotte.edu (L.M.)
† These authors contributed equally to this work.

Abstract: Despite substantial research efforts in developing high-voltage sodium-ion batteries (SIBs) as high-energy-density alternatives to complement lithium-ion-based energy storage technologies, the lifetime of high-voltage SIBs is still associated with many fundamental scientific questions. In particular, the structure phase transition, oxygen loss, and cathode–electrolyte interphase (CEI) decay are intensely discussed in the field. Synchrotron X-ray and neutron scattering characterization techniques offer unique capabilities for investigating the complex structure and dynamics of high-voltage cathode behavior. In this review, to accelerate the development of stable high-voltage SIBs, we provide a comprehensive and thorough overview of the use of synchrotron X-ray and neutron scattering in studying SIB cathode materials with an emphasis on high-voltage layered transition metal oxide cathodes. We then discuss these characterizations in relation to polyanion-type cathodes, Prussian blue analogues, and organic cathode materials. Finally, future directions of these techniques in high-voltage SIB research are proposed, including CEI studies for polyanion-type cathodes and the extension of neutron scattering techniques, as well as the integration of morphology and phase characterizations.

Keywords: sodium-ion batteries; cathode materials; high voltage; synchrotron X-ray scattering; neutron scattering

check for updates

Citation: Shipitsyn, V.; Jayakumar, R.; Zuo, W.; Sun, B.; Ma, L. Understanding High-Voltage Behavior of Sodium-Ion Battery Cathode Materials Using Synchrotron X-ray and Neutron Techniques: A Review. *Batteries* **2023**, *9*, 461. https://doi.org/10.3390/batteries9090461

Academic Editor: A. Robert Armstrong

Received: 21 July 2023
Revised: 29 August 2023
Accepted: 8 September 2023
Published: 11 September 2023

Copyright: © 2023 by the authors. Licensee MDPI, Basel, Switzerland. This article is an open access article distributed under the terms and conditions of the Creative Commons Attribution (CC BY) license (https://creativecommons.org/licenses/by/4.0/).

1. Introduction

To address global climate change by decreasing greenhouse gas emission, one of the decarbonization efforts is to widely use renewable clean energy such as solar, tidal, and wind energy. However, the integration of clean energy into the global grid network suffers from challenges in terms of stability and reliability due to the intermittent nature of renewable sources. The use of energy storage systems (ESSs) could mitigate this issue by storing electricity from renewable sources at off-peak times and discharging electricity at peak times [1,2].

Lithium-ion battery (LIB) technology is one of the most successful EESs and has been widely used in consumer electronics, electric vehicles (EVs), and electric grid networks [3–5]. However, the increasing demands in many energy sectors, including energy grid systems and EVs, highlight the need for dependable and cost-effective EESs that can serve as reliable alternatives to lithium and other critical elements such as cobalt [6,7]. Sodium-ion battery (SIB) technology has been considered as a viable option to supplement LIB

technology, especially in applications where high energy density is not a priority, such as grid ESSs [8,9]. This is due to the plentiful supply of sodium and the identification of cathode active materials containing inexpensive and abundant elements such as copper, iron, and manganese [10,11]. In addition, SIBs are closer to real-world applications than other "beyond-Li" battery chemistries including Zn, Mg, and Al due to the better kinetics of the monovalent working ion and the higher reversibility of working ions intercalation/de-intercalation compared to the stripping/plating process.

Common SIB cathode active materials (Figure 1) include: (1) layered transition metal oxides (Na_xMO_2, M = Co, Mn, Fe, Ni, Cu, etc.) [12–16]; (2) polyanionic compounds, such as phosphates (e.g., $Na_3V_2(PO_4)_3$ [17,18], $NaFePO_4$ [19,20]), fluoride phosphates (e.g., Na_2FePO_4F [21,22]), pyrophosphates (e.g., $Na_2FeP_2O_7$ [23,24]), and sulfates (e.g., $Na_2Fe_2(SO_4)_3$ [25,26]); (3) Prussian blue analogues (PBAs) compounds, such as $Na_xFeFe(CN)_6$ [27,28], $Na_xMnFe(CN)_6$ [29,30], and $Na_xNiFe(CN)_6$ [31,32]; (4) organic materials [8,33]. Classified by Delmas et al. [34,35], layered transition metal oxides have two structural forms including P_n and O_n, where P and O stands for prismatic and octahedral coordination, respectively, for the position of Na^+ in the edge-sharing MO_6 octahedra. n represents the number of transition metal layer repetitions within the stacking repeat unit. Polyanionic compounds are a broad category of compounds characterized by the presence of an anionic structural unit $(XO_m)^{n-}$ (P, S, and others) with a tetrahedral or octahedral structure [36,37]. Prussian blue analogues are compounds formed by the coordination of transition metal ions with a cyanide ion (CN^-) and have been widely used in many different applications due to their controllable structures [38]. Being different from inorganic materials, organic cathode materials consist of naturally light elements (C, H, O, etc.) with the unique advantages of stable redox characteristics and multi-electron reactions [33,39,40]. It is recognized that the increase in the operation voltage of these cathode materials is a feasible way of improving the energy density of SIBs.

Despite the growing expectations for SIBs, their practical application is restricted by their limited lifetime. Typically, cell degradation can originate from different parts, including the cathode, electrolyte, separator, and anode. The current challenges that SIB cathodes suffer from, especially at high voltage, can be summarized as follows [41]: (1) irreversible bulk phase transitions, which are accompanied by a large volume expansion and shrinkage as well as sluggish kinetics; and (2) surface-related degradation including surface instability in the air and interphasial side reactions between cathodes and electrolytes. A comprehensive and in-depth study of these fundamental issues is essential for developing high-voltage SIBs with an extended lifetime and higher energy density. Synchrotron X-ray and neutron scattering techniques significantly improve the efficiency and reliability of materials characterization by providing insight into the materials' bulk structure, electrode–electrolyte interphase evolution, and ionic motion dynamics [42–45]. Herein, a systematic and comprehensive summary of the synchrotron-X-ray- and neutron-scattering-based techniques used in characterizing high-voltage SIB cathode materials is introduced. We start with a brief overview of both synchrotron X-ray and neutron scattering techniques and their classifications. We then particularly highlight the fundamental scientific understanding of the high-voltage behavior of layered transition metal oxide SIB cathodes gained using these techniques. Polyanion-type cathodes, PBAs, and organic cathode materials are also discussed. Moreover, an outlook on the extension of synchrotron-X-ray- and neutron-scattering-based techniques regarding investigation into the cathode–electrolyte interphase (CEI), introduction of novel techniques (e.g., dark-field X-ray microscopy), and integration of morphology and phase characterizations is proposed for the study of high-voltage SIB cathode materials.

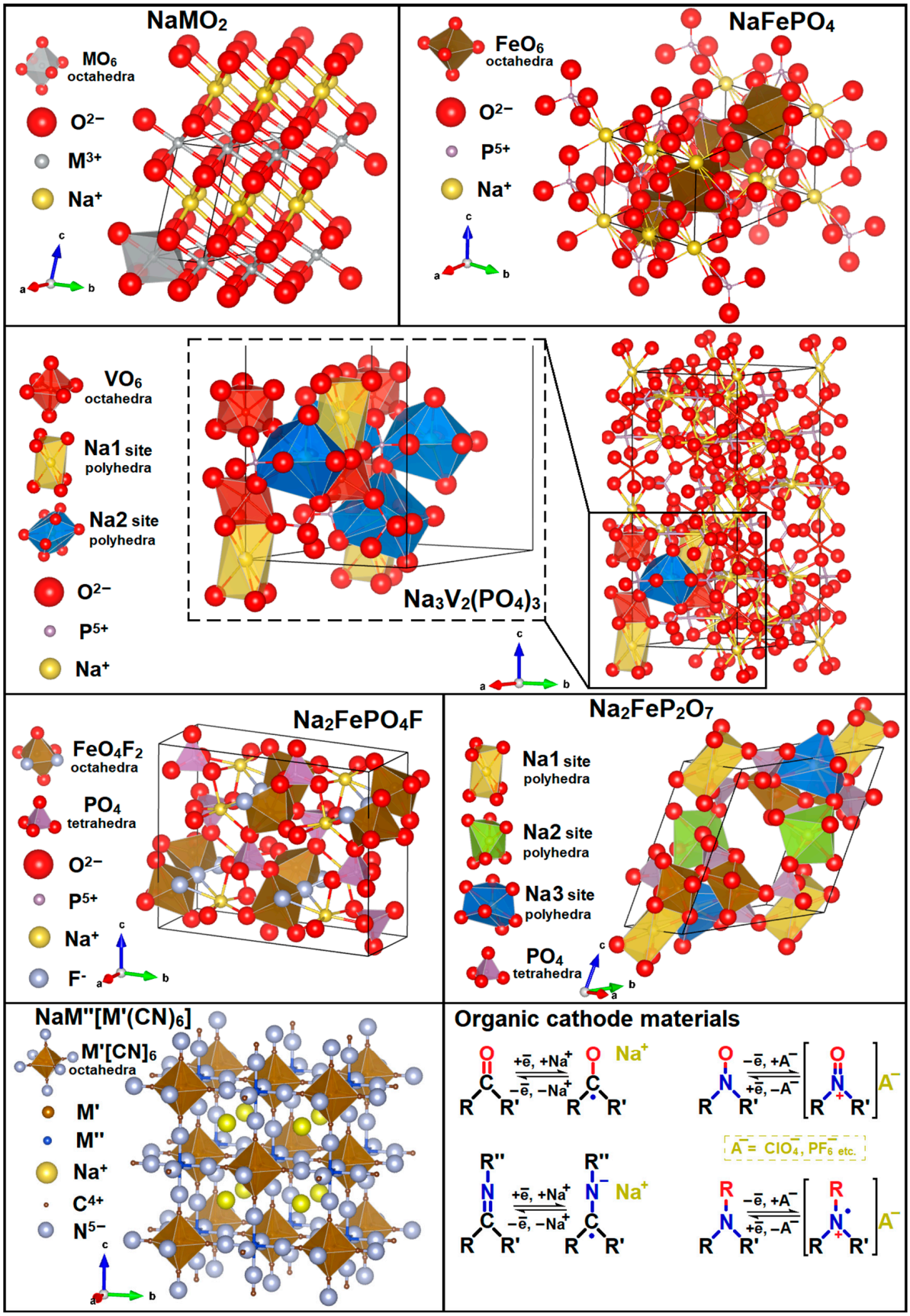

Figure 1. Common cathode active materials for SIBs.

2. Brief Overview of Synchrotron Radiation

According to classical electrodynamics, synchrotron radiation is generated as a narrow tangent to the path of charged particles with a relativistic speed [42]. Figure 2A shows a schematic of the basic components of a modern synchrotron facility. The acceleration of electrons begins by obtaining them from a source, such as a heated filament in an electron gun. Subsequently, these electrons are propelled forward through a linear accelerator (LINAC) before being introduced into a booster ring, where their acceleration continues. These electrons are then injected into the designated storage ring. Within this ring, bending magnet achromats are employed at arc sections to confine the electrons within a closed path. At the experimental hutch, the beamlines make use of the radiation emitted by insertion devices (IDs, e.g., wigglers, undulators) positioned at the straight sections between the arcs in the storage ring. The energy dissipated by the electrons due to the emission of synchrotron light is restored through radio frequency (RF) supplies.

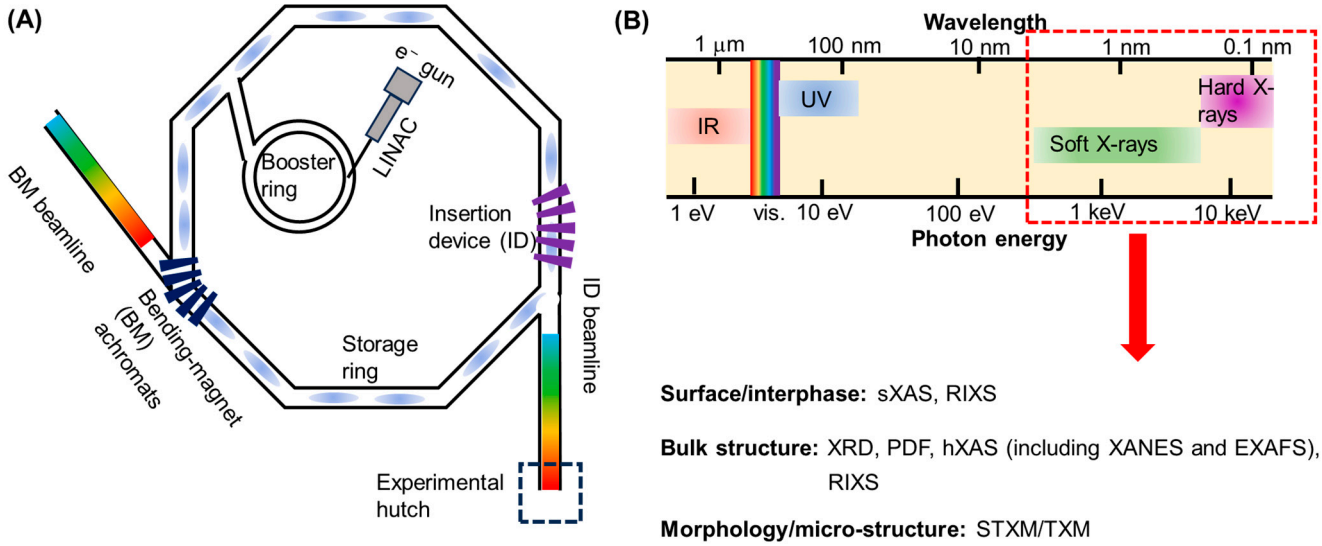

Figure 2. Schematics on the introduction of synchrotron techniques used in battery research. (**A**) A schematic of the basic components of a modern synchrotron facility. (**B**) Photon energy and the wavelength spectrum with common synchrotron X-ray techniques and their applications in battery research (IR—infrared; UV—ultraviolet; sXAS—soft X-ray absorption spectroscopy; XRD—X-ray diffraction; PDF—pair distribution function; hXAS—hard X-ray absorption spectroscopy; XANES—X-ray absorption near-edge structure; EXAFS—extended X-ray absorption fine structure; RIXS—resonant inelastic X-ray scattering; STXM/TXM—scanning/transmission X-ray microscopy).

While different photon energy ranges can be accessed through synchrotron radiation [42] (Figure 2B) and have been utilized for studying battery materials, this work only focuses on synchrotron-based X-ray techniques for the discussion and understanding of SIB cathode materials failure mechanisms. X-rays can be classified as hard, "tender", or soft according to their different photon energy range [42]. Hard X-rays have a photon energy range of a few kiloelectron volts (keV) to tens of keV while soft X-rays range from several tens of eVs to about 2 keV. The photon energy range of a "tender" X-ray is between the soft and hard X-ray ranges. Leveraging the different interactions between X-ray and matter, a combination of diverse X-ray techniques is preferred for disclosing detailed information on the surface, interphase, and bulk of battery materials (Figures 2B and 3).

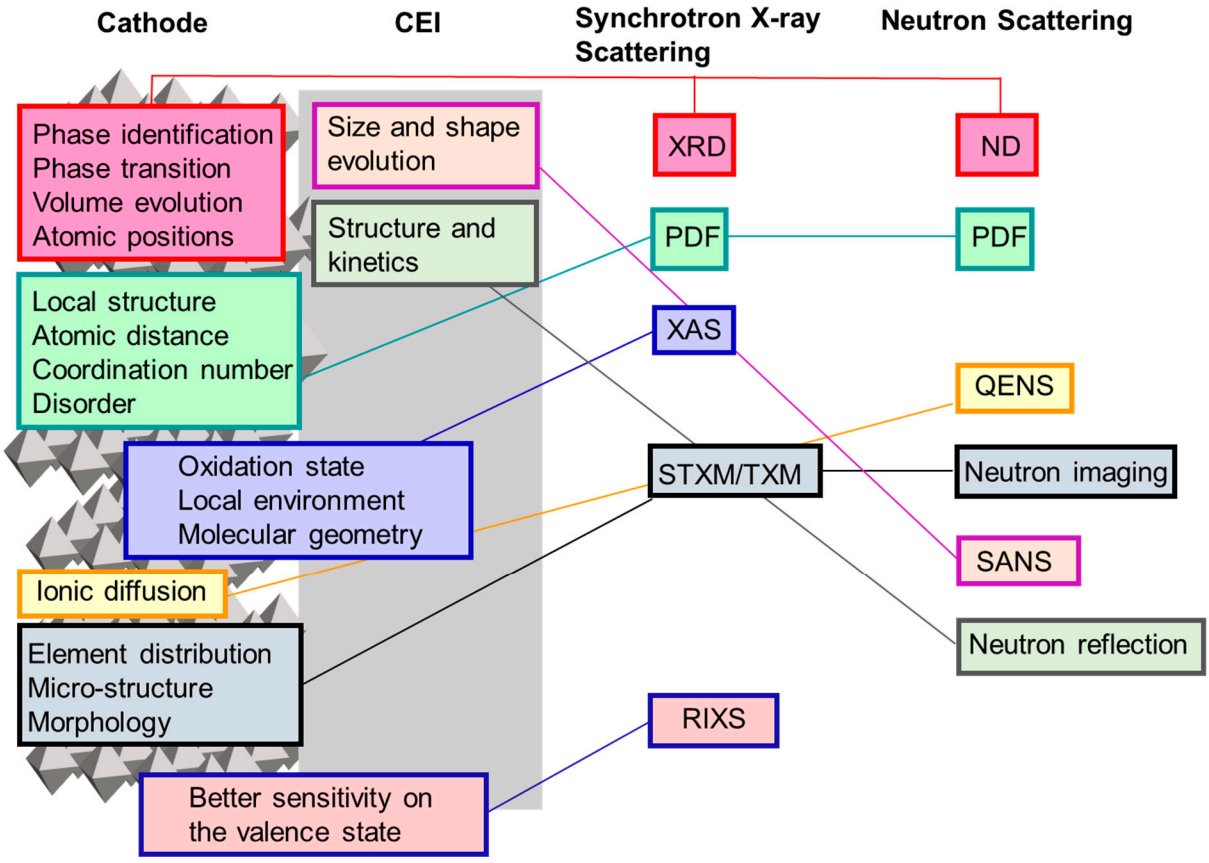

Figure 3. Overview of the capabilities of synchrotron X-ray and neutron scattering characterization techniques for the study of cathode materials and CEI in rechargeable battery systems.

3. Brief Overview of Neutron Technology

Neutrons, having no charge, possess a remarkable ability to penetrate through materials. Unlike X-rays, neutrons can traverse long distances without encountering significant scattering or absorption. Additionally, neutrons exhibit considerably lower levels of material damage compared to X-ray analysis [44,45]. These unique characteristics provide neutrons with distinct advantages for battery studies, offering complementary information to X-ray studies. Due to its high sensitivity to light elements, especially Li, Na, and O, the neutron technology is able to distinguish them from other heavy elements, such as Ni, Mn, and Fe, which are common elements in SIB cathode materials [46].

Some typical neutron scattering technologies are suitable for battery research including neutron diffraction (ND), small-angle neutron scattering (SANS), neutron total scattering combined with pair distribution function (PDF), inelastic neutron scattering (INS), quasi-elastic neutron scattering (QENS), and neutron imaging [46–49]. Leveraging Bragg's law, ND is used to study the crystal structures of materials at an atomic scale. PDF is a mathematical function that characterizes the probability of finding two atoms separated by a particular distance, which offers information about the spatial distribution of atom pairs. The combination of PDF with neutron total scattering is able to give insights into the structural characteristics and chemical environments of disordered materials. SANS is especially suitable for determining the structure of materials at the nanoscale in terms of the size, shape, and spatial arrangement of particles. QENS provides insights into the dynamic behavior (e.g., motion and diffusion) of atoms and molecules within materials by examining the energy and momentum transfer of neutrons during scattering. By offering enhanced penetration and elemental contrast capabilities, neutron imaging allows for the visualization of certain elements' distribution. Typically, these neutron scattering

techniques can serve as complementary support for synchrotron X-ray characterizations to obtain a comprehensive understanding of high-voltage cathode behavior (Figure 3).

4. Layered Oxide Cathode Materials

The sodium-based layered transition metal oxide Na_xMO_2 (M: transition metal) consists of stacked edge-sharing MO_6 octahedral sheets. In accordance with Delmas' notation [13,50], Na_xMO_2 can be categorized into O3 and P2 structures. In the O3 structure, the Na^+ ions are located in octahedral sites, whereas, in the P2 structure, they occupy prismatic sites. Typically, Na_xMO_2 can be operated at a relatively high operating voltage based on transition metal redox couples (e.g., Ni^{2+}/Ni^{4+}) [37,51,52]. In addition, the participation of anionic (oxygen) redox activity leads to extra capacities at higher voltages [37]. However, it is challenging to realize a long-lifetime high-voltage SIB with Na_xMO_2 (Table 1) partially due to the degradation processes at the cathode side including structural transitions, oxygen loss, and interphasial reactions. Here, we discuss the use of synchrotron X-ray scattering and neutron scattering techniques to understand these Na_xMO_2 failure mechanisms and move towards addressing them.

Table 1. A summary of the selected electrochemical performance of high-voltage SIBs with Na_xTMO_2.

Material	Electrolyte	Temperature	Cycling Rate	Voltage Range	Cycling No. Until 80% Capacity Retention	Ref.
$Na_{0.5}Cu_{0.15}Ni_{0.2}Mn_{0.65}O_2$/Na	1M $NaClO_4$ in PC + 5%FEC	Room temperature	1000 mA/g	3–4.2 V	1000	[53]
$Na_{0.66}Ni_{0.26}Zn_{0.07}Mn_{0.67}O_2$/Na	1M $NaClO_4$ in PC + 2%FEC	Room temperature	12 mA/g	2–4.4 V	30	[54]
$NaxNi_{1/3}Co_{1/3}Mn_{1/3}O_2$/Na	1M $NaPF_6$ in PC + 2%FEC	Room temperature	0.5C	2–4.4 V	100	[55]
$Na_{0.67}Ni_{0.23}Mn_{0.67}Mg_{0.1}O_2$/Na	1M $NaClO_4$ in PC + 5%FEC	Room temperature	0.1C	2–4.5 V	100	[56]
$Na_{2/3}[(Ni_{0.5}Zn_{0.5})_{0.3}Mn_{0.7}]O_2$/Na	0.5M $NaPF_6$ in PC + 2%FEC	Room temperature	0.1C	2.3–4.6 V	>200	[57]
$Na_{0.6-x}Ca_xNi_{1/3}Mn_{1/3}Co_{1/3}O_2$/Na	1M $NaPF_6$ in EC/DEC 1/1 + 3%FEC	Room temperature	200 mA/g	2.5–4.2 V	~100	[58]
Ru-substituted $Na_{0.6}MnO_2$/hard carbon	1M $NaClO_4$ in PC + 5%FEC	Room temperature	100 mA/g	1.5–4.4 V	50	[59]
$Na_{0.67}Ni_{0.19}Cu_{0.14}Mn_{0.52}Ti_{0.15}O_2$/Na	1M $NaClO_4$ in EC/DEC 1/1 + 5%FEC	Room temperature	0.1C	2–4.5 V	100	[60]

Structural transitions: Phase transition of cathode materials, especially at high voltage, can be detrimental to the cell performance due to the potential changes of crystal structure and lattice parameters, which could result in the following: cracking, pulverization, a loss of active material, and inferior kinetics of ion transportation [37]. Substitution and doping are widely used to suppress phase changes of Na_xMO_2 during cell operation at a high voltage, especially when synchrotron X-ray [15,55,61–66] and neutron scattering techniques [16,67–69] are used to obtain a comprehensive understanding of their effects. Synchrotron X-ray diffraction (XRD) and ND are typically used for characterizing phase changes of Na_xMO_2 as a function of potential. Tapia-Ruiz et al. [62] investigated the effects of Mg substitution on P2-type $Na_{2/3}Ni_{1/3-x}Mg_xMn_{2/3}O_2$ ($0 < x < 0.2$) with XRD to realize the suppression of the O2 phase by the formation of an OP4 phase above 4V. ND was utilized to explain the substituted sites of Ni^{2+} from ordered $[(Ni^{2+}/Mn^{4+})O_6]$ honeycomb units by Mg^{2+}. Liu et al. [16] studied the structure of a P3-type layered oxide $Na_{0.5}Ni_{0.25}Mn_{0.75}O_2$ cathode, especially the nature of the high-voltage phase above 4 V, using in situ neutron diffraction (Figure 4A). They clearly showed the phase above 4 V (O3s phase) has a dramatically shorter interlayer distance when all sodium has been removed. The substitution or doping elements could be involved in the redox process and affect charge compensation mechanisms, which can be elaborated using synchrotron X-ray absorption spectroscopy (XAS). Liu et al. [15] developed the Fe/Ti co-substitution strategy to suppress P2–O2 phase transition and Na^+/vacancy ordering at high voltages for P2–$Na_{2/3}Ni_{1/3}Mn_{2/3}O_2$ cathode material. They demonstrated the incorporation of an $Fe^{3+/4+}$ redox couple in the charge compensation using ex situ XAS (Figure 4B). XAS can also be

used to study local atomic structure because it provides information on the short-range order of atoms surrounding the absorbing atom. With detailed analysis, one can determine the types of atoms surrounding the absorbing atom, bond distances, and coordination numbers. Leveraging extended X-ray absorption fine-structure (EXAFS) spectroscopy combined with fitting analysis, Bhange et al. [61] revealed unique local structure changes around Ni atoms due to the honeycomb ordering and size mismatch between Ni^{2+} and Bi^{5+} cations (Figure 4C).

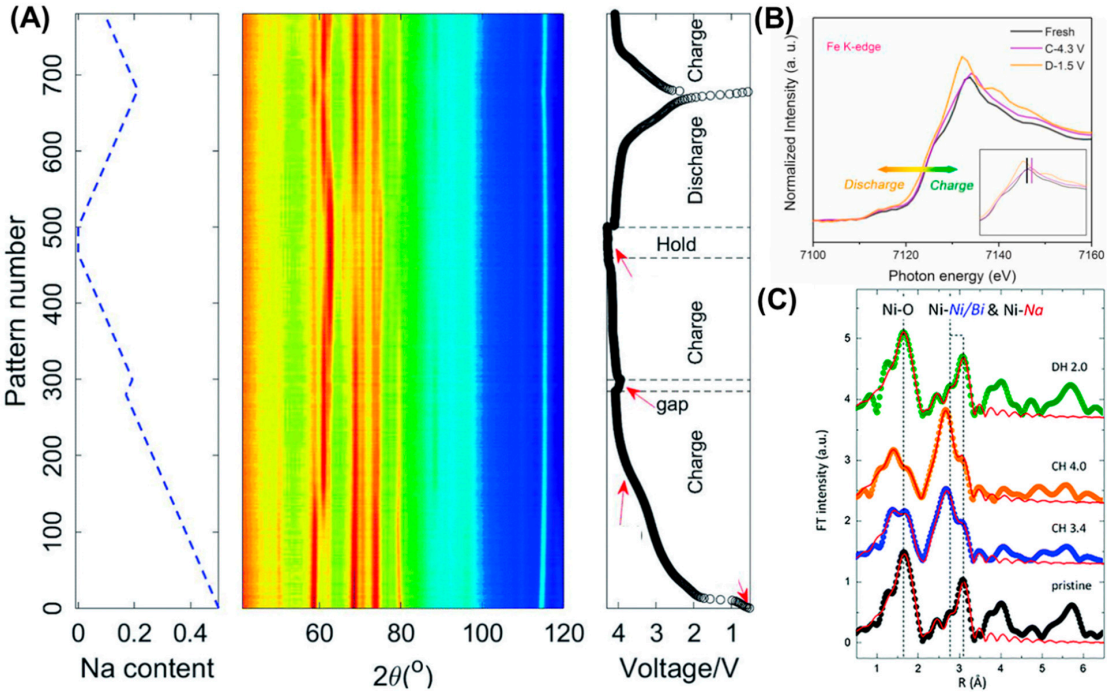

Figure 4. Examples of synchrotron X-ray or neutron scattering techniques used in characterizing structure transitions of Na_xMO_2 cathode materials. (**A**) In situ ND patterns of the $Na_{0.5}Ni_{0.25}Mn_{0.75}O_2$-hard carbon pouch cell collected while cycling at 10 mA g^{-1}. Reproduced from ref [16], copyright 2020 Royal Society of Chemistry. (**B**) Ex situ Fe K-edge XANES spectra for $Na_{0.66}Ni_{0.23}Fe_{0.1}Mn_{0.57}Ti_{0.1}O_2$ electrode. Reproduced from ref. [15], copyright 2021 Elsevier. (**C**) Ni K-edge EXAFS spectra of $Na_3Ni_2BiO_6$ samples at different states of charge. Reproduced from ref. [61], copyright 2016 Royal Society of Chemistry.

Irreversible oxygen redox activity: As a special case of structural transition, oxygen loss, is discussed here as an independent section because of its universality for Na_xMO_2 cathodes when charging to high voltage. To further increase the energy density of SIBs, it is urgent to utilize the extra capacity caused by the oxygen redox activity. However, large, irreversible capacity accompanied by oxygen loss and voltage decay typically occurs after the first charge process [70]. Thus, to develop Na_xMO_2 cathode materials with highly reversible oxygen redox activity, fundamental studies of the redox reactions are required from the perspective of charge compensation mechanisms and rational materials design principles. X-ray absorption near-edge structure (XANES) spectroscopy has been demonstrated to be a reliable method of determining the redox contribution from oxygen (Figure 5A) [57,71,72]. Structural modification using element substitution [73–75] or doping [12,14,72] has been reported to suppress oxygen redox activity and decrease voltage hysteresis. Ji et al. [73] reported that the substitution of Mg and Zn in a cathode material, $Na_{0.67}Mg_{0.1}Zn_{0.1}Mn_{0.8}O_2$, could deliver an ultra-high capacity of ~233 mAh/g at 0.1 C by preventing the oxygen loss. Combining neutron PDF (Figure 5B) and resonant inelastic X-ray scattering (RIXS, Figure 5C), they illustrated the migration of Mg^{2+} and Zn^{2+} out of the layer with consequent vacancy cluster structures that could trap O_2 molecules when

fully charged. Yu et al. [72] improved the reversibility and stability of O^{2-} by tuning the Na–O–TM structure to increase the energy level of the O 2p electronic state using a Zr^{4+} doping strategy in an O3-type $NaMn_{1/3}Fe_{1/3}Ni_{1/3}O_2$ cathode material, which was proved by the O K-edge ex situ XAS results. The oxygen loss in oxygen redox cathodes can also be avoided by forming certain types of superstructures in the transition metal layers that can suppress transition metal migration [70]. House et al. [76] demonstrated that the formation of ribbon superstructure in $Na_{0.6}[Li_{0.2}Mn_{0.8}]O_2$ could inhibit Mn disorder, O_2 formation, and voltage hysteresis by synchrotron XAS (Figure 5D).

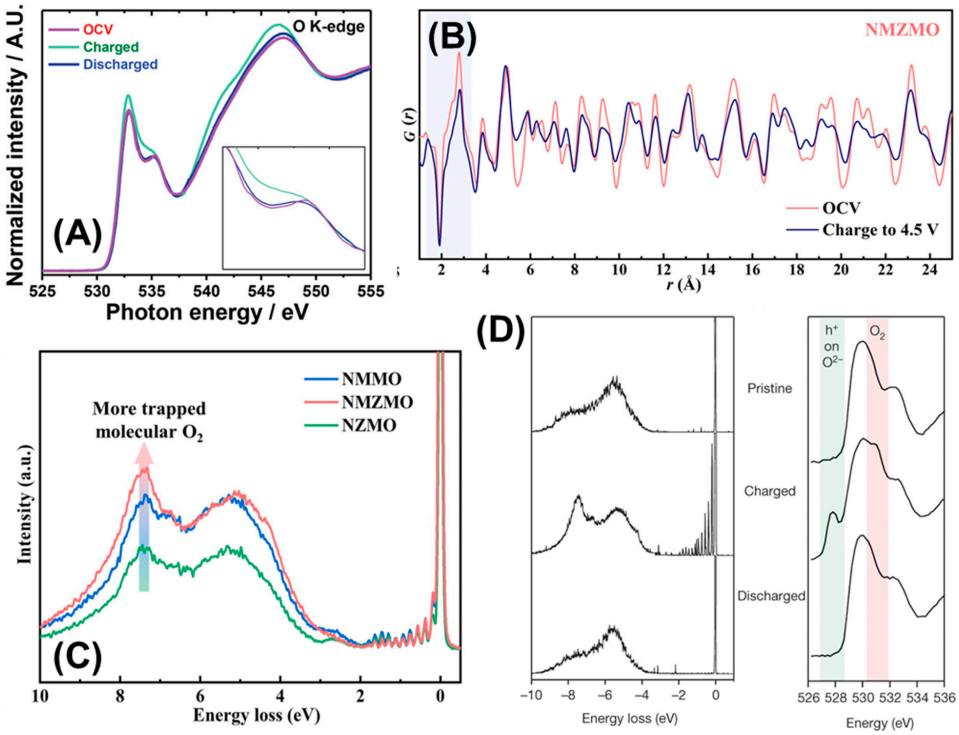

Figure 5. Examples of synchrotron X-ray or neutron scattering techniques used in characterizing oxygen redox activity of Na_xMO_2 cathode materials. (**A**) O K-edge of ex situ XANES spectra for P2-$Na_{2/3}[(Ni_{0.5}Zn_{0.5})_{0.3}Mn_{0.7}]O_2$. Reproduced from ref. [57], copyright 2020 Wiley. (**B**) Neutron PDF patterns of $Na_{0.67}Mg_{0.1}Zn_{0.1}Mn_{0.8}O_2$ collected at the OCV and 4.5 V. The low r region labeled by a light-blue square was analyzed to obtain information on the shrinkage of the O–O bond length. (**C**) O K-edge RIXS measurements taken on $Na_{0.67}Mg_{0.2}Mn_{0.8}O_2$, $Na_{0.67}Zn_{0.2}Mn_{0.8}O_2$, and $Na_{0.67}Mg_{0.1}Zn_{0.1}Mn_{0.8}O_2$ charged to 4.5 V at 531 eV. Reproduced from ref. [73], copyright 2023 Elsevier. (**D**) O K-edge XAS (right panel) and RIXS spectra (left panel) recorded at an excitation energy of 531 eV for ribbon-ordered $Na_{0.6}[Li_{0.2}Mn_{0.8}]O_2$ at different states of charge (i.e., pristine, 4.5 V, and 2 V). Reproduced from ref. [76], copyright 2019 Nature Springer.

Cathode-electrolyte interphasial reactions: It has been reported that cathode–electrolyte interphasial reactions can compromise SIBs lifetime by causing transition metal reduction and dissolution, electrolyte oxidation, heterogeneous surface reconstruction, and intragranular nanocracks [11,77,78]. However, the complicated chemical species and some native surface film (e.g., NaOH, Na_2CO_3) on cathode surfaces make it difficult to discern the products from the electrochemical process [79]. Here, we summarize the use of synchrotron X-ray techniques to diagnose the interphasial chemistries with the hope of providing scientific insights into stabilizing the interphase through cathode modification, electrolyte design, and artificial interphase fabrication. Soft XAS is a common technique used to investigate the surface chemical environments with both fluorescence yield (FY) and total electron yield (TEY) modes. Comparing the FY and TEY spectra of the same element, one can study the depth-dependent chemical changes because FY mode is used for probing the

subsurface (≈50 nm) while TEY mode is used for studying the surface (≈10 nm) [77,80,81]. Mu et al. [77] realized electrolyte oxidation on the cathode surface by revealing a lower Ni oxidation state at the surface using TEY mode compared to FY mode at all states of charge (Figure 6A). Being similar to conventional XPS, synchrotron-based hard X-ray photoelectron spectroscopy (HAXPES) is able to provide interphasial chemical information by analyzing the electronic properties of materials with an extended penetration depth and improved sensitivity. Doubaji et al. [82] demonstrated the interphasial chemistries evolution on the surface of $Na_xCo_{2/3}Mn_{2/9}Ni_{1/9}O_2$ during cycling using HAXPES (Figure 6B). Transmission X-ray microscopy (TXM), a non-destructive imaging technique, allows for the tracking of transition metal migration, which can be caused by interphasial reactions, through visualizing and analyzing the three-dimensional (3D) distribution of transition metal cations [83,84]. For example, Rahman et al. [83] confirmed the Mn migration to the $Na_{0.9}Cu_{0.2}Fe_{0.28}Mn_{0.52}O_2$ particle surface during cycling by using TXM (Figure 6C). Although there are rare reports discussing the use of neutron scattering technology in studying CEI, there is plenty of scope for applying this technique in this area. We discuss it in the perspective section.

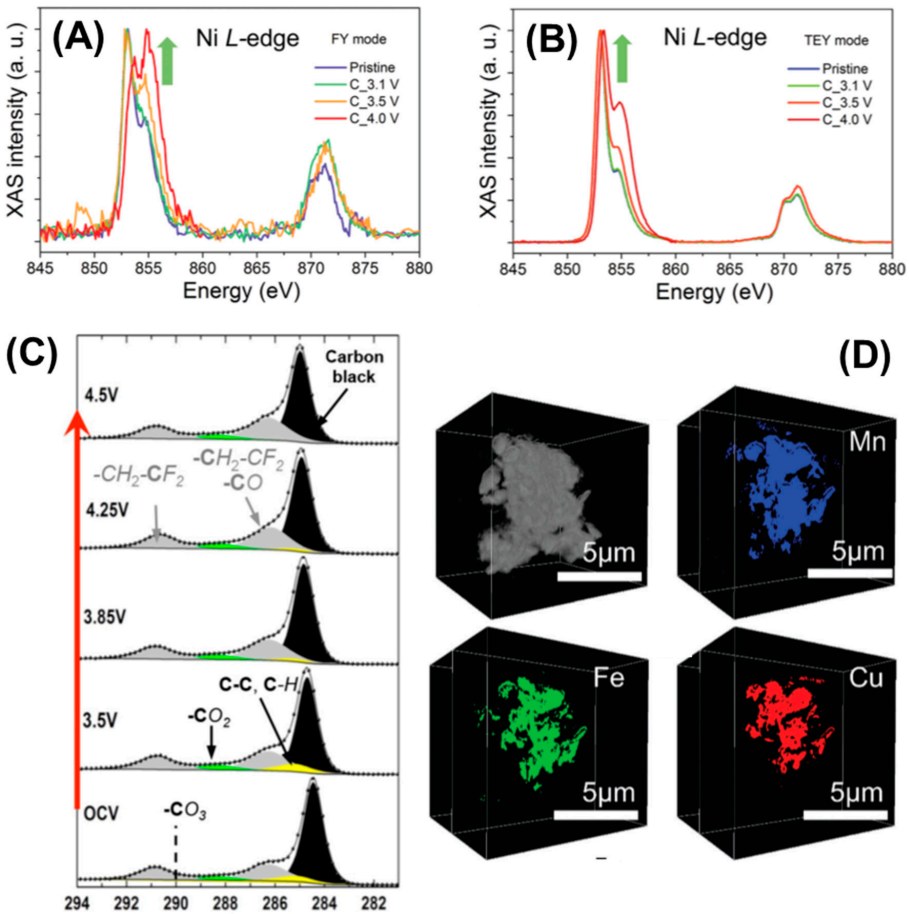

Figure 6. Examples of synchrotron X-ray techniques used in characterizing the Na_xMO_2 cathode–electrolyte interphasial chemical process. Soft XAS spectroscopy of Ni L-edge in FY mode (**A**) and TEY mode (**B**) of the O3–$NaNi_{1/3}Fe_{1/3}Mn_{1/3}O_2$ cathode at different charge states. Reproduced from ref. [77], copyright 2018 Wiley. (**C**) Neutron PDF patterns of $Na_{0.67}Mg_{0.1}Zn_{0.1}Mn_{0.8}O_2$ collected at the OCV and 4.5 V. (**C**) C1s HAXPES spectra for $Na_xCo_{2/3}Mn_{2/9}Ni_{1/9}O_2$ at different voltage stages during charge. Reproduced from ref. [82], copyright 2016 Wiley. (**D**) 3D morphology of the $Na_{0.9}Cu_{0.2}Fe_{0.28}Mn_{0.52}O_2$ particle after cycling rendered from single-energy TXM data. Reproduced from ref. [83], copyright 2018 Royal Society of Chemistry.

5. Polyanion Compounds

Polyanion-type compounds, built with $(XO_4)^{n-}$ (X = B, S, P, Si, etc.) units or their derivatives, have also attracted substantial research interest [36,37]. They are able to exhibit higher operating potentials, which is due to the inductive effect of polyanion groups [85]. The strong X–O covalent bonds dramatically improve the stability of lattice oxygen, thus increasing the thermal stability of polyanion-type cathode materials compared to layered oxide cathodes. However, polyanion-type cathode materials have a relatively low gravimetric specific capacity because of the heavy polyanion groups' presence. To increase the SIBs' energy density, it is important to explore high-voltage polyanion materials (e.g., phosphates, fluoride phosphates, pyrophosphates) to obtain more capacity. However, polyanion cathode materials can suffer from structural transition and severe interphasial reactions at high voltages, thus decreasing cell lifetime (Table 2). In addition, it is difficult to understand the charge compensation mechanisms because the transition metal redox couple varies significantly with different structures and polyanionic groups.

Table 2. A summary of the selected electrochemical performance of high-voltage SIBs with polyanion cathodes.

Material	Electrolyte	Temperature	Cycling Rate	Voltage Range	Cycling No. Until 80% Capacity Retention	Ref.
$NaVOPO_4$//Na	1M $NaClO_4$ in EC/DEC 1/1	Room temperature	0.5C	2–4.2 V	1000	[86]
$Na_3V_2(PO_4)_2F_3$/Na	1M $NaClO_4$ in EC/DEC 1/1 + 5%FEC	Room temperature	10C	2.5–4.5 V	>1000	[87]
$Na_2Fe(C_2O_4)SO_4 \cdot H_2O$/Na	1M $NaClO_4$ in PC + 3%FEC	Room temperature	0.2C	1.7–4.2 V	500	[88]
$Na_{1.4}Fe_{1.3}P_2O_7$/Na	1M $NaClO_4$ in EC/PC 1/1 + 5%FEC	Room temperature	1C	1.5–4.2 V	650	[89]
$Na_2VTi(PO_4)_2F_3$/Na	$NaPF_6$ in PC/EC/DMC 1/1/1	Room temperature	0.1C	3–4.4 V	>100	[90]
$Na_3MnZr(PO_4)_3$/Na	1M $NaClO_4$ in PC/FEC 9/1	Room temperature	0.5C	2.5–4.2 V	>500	[91]
$Na_4MnCr(PO_4)_3$/Na	1M $NaClO_4$ in PC/FEC 9/1	Room temperature	10C	1.5–4.3 V	>500	[92]

To address these challenges, researchers have utilized state-of-the-art characterization techniques to investigate the micro/macro structure, chemical composition changes, and sodium storage mechanism of polyanion-type cathode materials. The use of ND (Figure 7A) and synchrotron XRD (Figure 7B) has been widely reported in the illustration of the structural transition of polyanion-type cathode materials, especially during high-voltage operation [93–97]. Leveraging in situ synchrotron XRD, Chen et al. [93] revealed a near-zero volume change for N-doped graphene-oxide-wrapped $Na_3V(PO_3)_3N$ cathode materials during cycling. Wang et al. [94] developed a new cathode, $Na_4MnCr(PO_4)_3$, with a high specific capacity of 130 mAh g^{-1}. Its structural evolution with a sequence of single phase, two phases, and single phase during discharge was confirmed by the synchrotron XRD data. Synchrotron-based XAS has also been utilized to study transition metal redox activity to understand the charge compensation mechanisms for high-voltage polyanion-type cathode materials (Figure 7C) [88,93,98]. Kawai et al. [98] demonstrated the activity of a Cr^{4+}/Cr^{3+} redox couple in $Na_{3-x}Cr_2(PO_4)_3$ at 4.5 V vs. Na/Na^+ using Cr K-edge XANES spectra. When more transition metal redox couples were involved in the $Na_4MnCr(PO_4)_3$ cathode, Zhang et al. [96] were able to reveal the underlying mechanism of the Mn^{2+}/Mn^{3+}, Mn^{3+}/Mn^{4+}, and Cr^{3+}/Cr^{4+} redox couples via XANES spectroscopy.

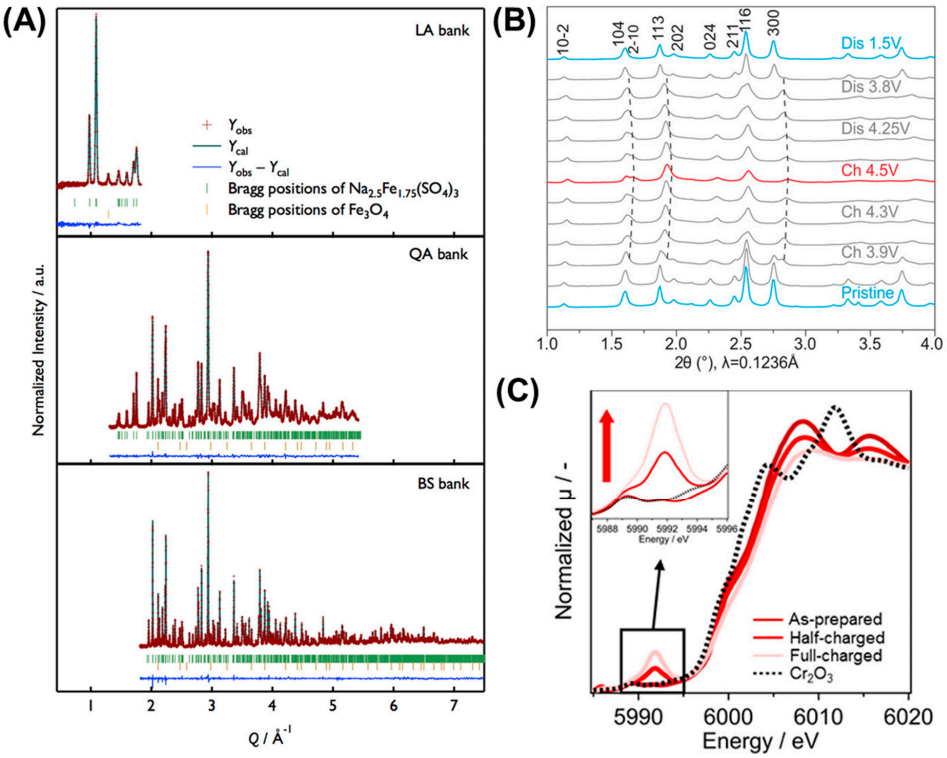

Figure 7. Examples of synchrotron X-ray techniques used in characterizing polyanion-type cathode materials. (**A**) Observed and calculated scattering intensity versus scattering vector Q for ND pattern of $Na_{2.5}Fe_{1.75}(SO_4)_3$ at 620 K. Reproduced from ref. [95], copyright 2016 American Chemical Society. (**B**) Ex situ synchrotron XRD patterns of $Na_4MnCr(PO_4)_3$ at various states of charge. Reproduced from ref. [94], copyright 2020 Wiley. (**C**) Cr K-edge XANES spectra of $Na_3Cr_2(PO_4)_3$/acetylene black electrode in the first charging process. Reproduced from ref. [98], copyright 2018 American Chemical Society.

To develop high-voltage, friendly electrolyte systems for polyanion-type cathode materials, there have been many studies discussing the CEI [99–104]. However, synchrotron X-ray and neutron scattering techniques have not been widely used in investigating the interphasial chemical evolutions for polyanion-type cathode materials. We discuss their potential applications in this area in the perspective section.

6. Prussian Blue Analogue and Organic Materials

Due to the advantages of excellent redox activity, low cost, and elemental Earth abundance, Prussian blue (PB), its analogues (PBAs), and organic materials have been widely investigated as promising cathode active materials for SIBs. However, their average working voltage is not as satisfactory as the one from transition metal oxides and polyanionic compounds. To further improve cell energy density, recently emerging efforts have been devoted to increasing the working voltage of PBAs and organic cathode materials from the perspective of tuning the materials' structure [105–107]. Although synchrotron X-ray and neutron scattering have less often been used with a focus on investigating high-voltage PBAs and organic cathodes, it is urgent to highlight the application of these advanced characterizations in these existing cathode chemistries with the hope of increasing the use of these techniques in future high-voltage PBAs and organic cathodes.

PBAs, typically represented by a chemical formula of $A_xM_1[M_2(CN)_6]_y\square_{1-y}\ zH_2O$, consist of more than 100 family members with different crystal phases [38]. Here, A represents an alkali metal while M1 and M2 represent transition metals. Typically, these transition metals are bonded with a $C{\equiv}N^-$ anion to form a three-dimensional open structure for hosting working ions (i.e., A). The sign of "□" represents the structural vacancy associated with the lack of $M_2(CN)_6$ group. The electrochemical activity with electron transfer of

PBA cathode materials is typically associated with the valence change of M_1 and M_2. Due to the crystallinity and the involvement of transition metals, synchrotron XRD and XAS are typically used in characterizing PBAs to investigate bulk structure changes and redox mechanisms, respectively [108–111]. To extend the cell lifetime, it is important to eliminate crystal water from PBAs. Wang et al. [111] illustrated phase transformation for a dehydrated $Na_{2-x}FeFe(CN)_6$ sample during cycling in situ by synchrotron XRD (Figure 8A). Seok et al. [110] studied the structure of a PBA using synchrotron XRD when iron was substituted with nickel (PBN). They demonstrated that the addition of nickel could dramatically decrease the volumetric expansion, thus improving cycling stability. In addition, the added nickel was electrochemically inactive, which was proved by the XANES data (Figure 8B). X-ray total scattering combined with the PDF technique has also been used to study the local structure and coordination geometry of PBAs. Xu et al. [112] identified the structure difference in a short range (r < 10 Å, Figure 8C) between cubic structured nickel hexacyanoferrate (NiHCF) and monoclinic NiHCF using synchrotron X-ray total scattering with PDF analysis. This could have been caused by the lattice distortion and Fe−C≡N−Ni skeleton twisting in the monoclinic phase. As a complementary technique, ND combined with refinement has been used in characterizing the bulk structure of PBAs. Using ND, Peng et al. [113] identified the structure of a rust-derived Prussian blue as an SIB cathode material with the Na^+ occupying the 8c and 24d positions. Leveraging ND with the refinement of the oxygen occupancies, Nielsen et al. [114] reported that water molecules do not induce phase transitions for $Na_2Fe\,[Fe(CN)_6]\cdot zH_2O$. Other neutron scattering techniques also need to be applied in studying PBAs to obtain more insights into further high-voltage chemistries, which are discussed in the perspective section.

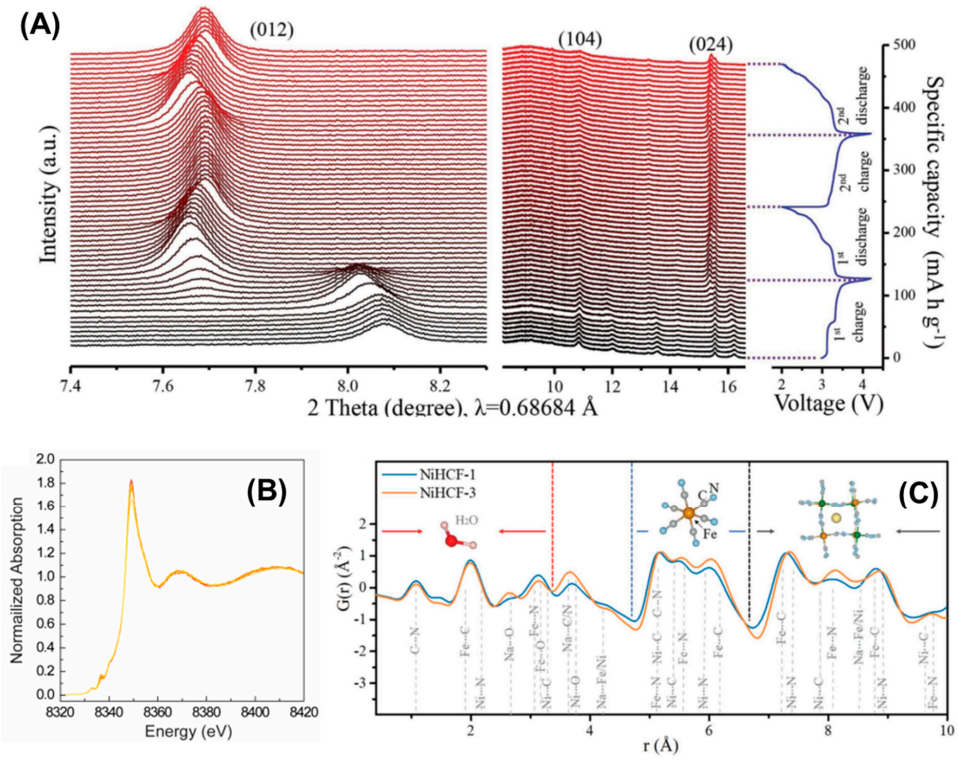

Figure 8. Examples of synchrotron X-ray techniques used in PBA SIB cathode materials. (**A**) (012), (104), and (024) reflection planes from in situ synchrotron XRD of the high-temperature-treated $Na_{2-x}FeFe(CN)_6$ sample. Reproduced from ref. [111], copyright 2022 Wiley. (**B**) Operando XANES spectra at Ni K-edge of PBN during discharging process. Reproduced from ref. [110], copyright 2020 American Chemical Society. (**C**) PDF pattern of cubic (purplish blue) and monoclinic (orange) structured NiHCF. Reproduced from ref. [112], copyright 2019 Wiley.

Organic cathode materials, typically consisting of light elements (e.g., C, H, O, N), can be divided into n type, p type, and bipolar type according to their different redox-active units or moieties with redox mechanisms [33,39]. Typically, many n-type organic materials involve an initial reduction process that leads to the formation of a negatively charged state to combine with metal cations. Usually p-type organic materials undergo an oxidation process to combine with anions in the electrolytes. By incorporating the two characteristics described above, bipolar-type organic materials exhibit the capability to undergo either oxidation or reduction processes. Due to the lack of redox activities from transition metals, the use of synchrotron X-ray techniques to characterize typical organic cathodes has not attracted substantial interest. However, the proper use of synchrotron X-ray combined with ab initio molecular dynamics (MD) simulations is also able to illustrate short-range structural features of organic materials at different states of charge. Kuan et al. [115] reported a novel small molecule, hexaazatrianthranylene embedded quinone (HATAQ, Figure 9A), as an SIB cathode material with 99% capacity retention over 5000 cycles at a high rate of 60 A g^{-1}. Leveraging ex situ synchrotron total X-ray scattering measurements (Figure 9B) with theoretical modeling, they illustrated the sodium storage mechanism by elaborating the appearance of Na–C, Na–O, and Na–N correlations.

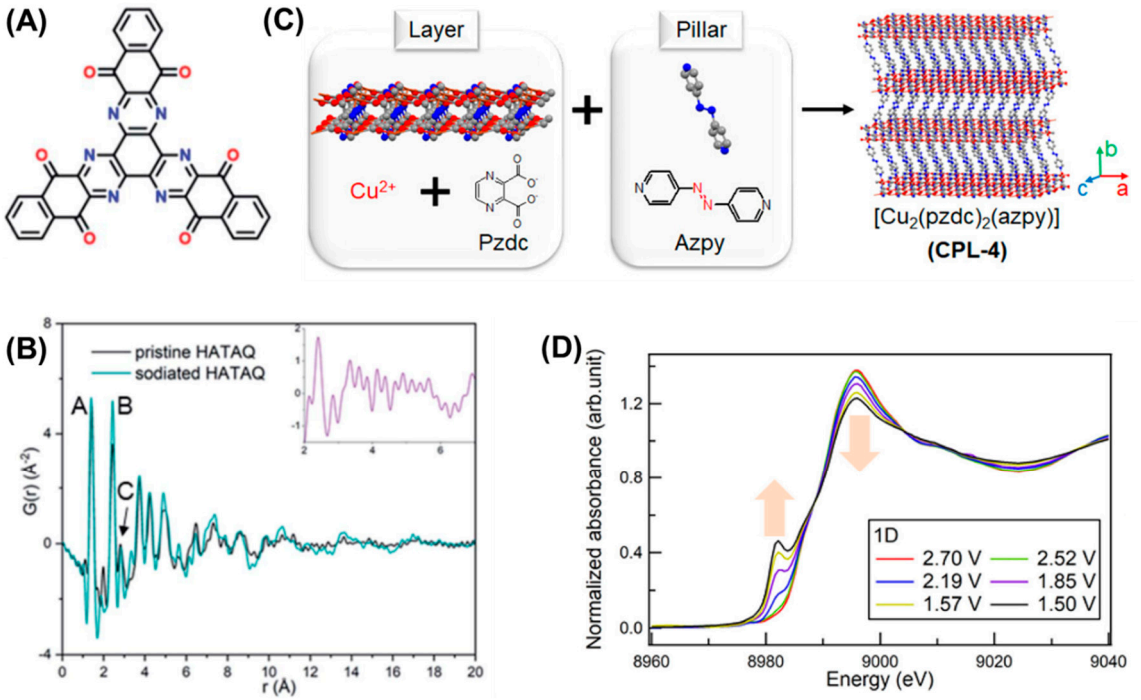

Figure 9. Examples of synchrotron X-ray techniques used in organic SIB cathode materials. (**A**) Chemical structure of the small-molecule HATAQ; (**B**) synchrotron X-ray PDFs of pristine and sodiated HATAQ. Reproduced from ref. [115], copyright 2022 Royal Society of Chemistry. (**C**) Schematic representation of the pillar-layered structures of CPL-4; (**D**) operando Cu K-edge XANES spectra of the CPL-4 cathode during the first discharging process. Reproduced from ref. [116], copyright 2022 American Chemical Society.

To improve the working potential of organic cathodes, it is feasible to combine organic redox species with transition-metal-containing compounds. Shimizu et al. [116] investigated CPL-4 ([Cu_2(pzdc)$_2$(azpy)], pzdc = pyrazine-2,3-dicarboxylate, azpy = 4,4-azopyridine, Figure 9C) as an SIB cathode material, which is a combination of aromatic azo compounds with metal carboxylates. The Cu element in this cathode material facilitates the use of synchrotron X-ray characterization to illustrate the redox reaction mechanism. The operando Cu K-edge XANES spectra (Figure 9D) were collected to demonstrate the

reversible redox reaction of Cu^{2+}/Cu^{+}. The use of neutron characterization in organic cathode materials needs to be extended, which is discussed in the perspective section.

7. Conclusions and Perspectives

High-voltage materials have shot to notability as a promising research area for SIBs because of their advantage of improving cell energy density with Earth-abundant elements. However, they face several serious problems such as bulk structure transition, lattice oxygen irreversibility, and cathode–electrolyte interphase evolution. Different strategies have been performed to improve the performance of high-voltage SIB cathode materials, such as element substitution or doping, rational electrolyte design, and artificial interphase fabrication. Simultaneously, state-of-art characterization techniques need to be applied to comprehensively understand the relationship between electrochemical performance and the evolution of the bulk and interphase during high-voltage operation.

In this review, synchrotron-X-ray- and neutron-scattering-based characterization techniques applied in high-voltage SIB cathode materials with both ex situ and in situ methods are summarized systematically. These characterization techniques are related to crystal structure, chemical composition and distribution, and valence state changes. The crystal-structure-related techniques (e.g., XRD, ND, PDF) have been proven as powerful tools to track the phase transformation and local atomic structures during the electrochemical processes. Composition- and valence-state-related techniques, such as RIXS, HAXPES, and XAS, can provide valuable information about potential reaction pathways and charge compensation mechanisms. Morphology- and element-distribution-related techniques, such as TXM, are able to provide detailed information about the internal structure, morphology, and elemental distribution of materials at the micrometer or nanometer scale. Despite the advantages of these characterizations mentioned above, there is plenty scope to use these characterizations to address the challenges of high-voltage SIB cathodes, especially when synchrotron X-ray and neutron scattering techniques are updated. We would like to summarize a few specific and practical directions for further research using synchrotron-X-ray- and neutron-scattering-based techniques (Scheme 1).

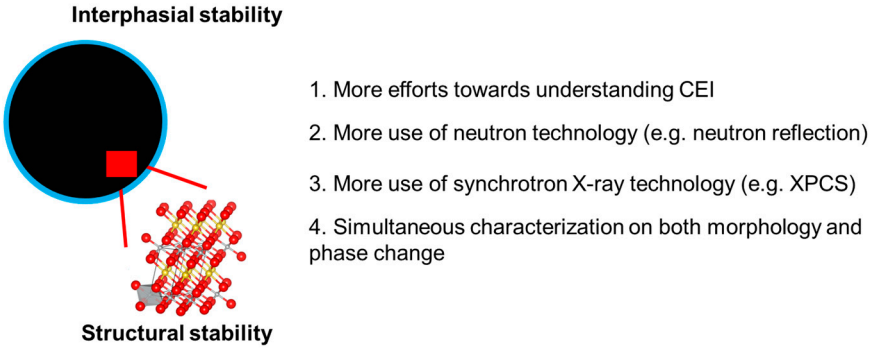

Scheme 1. Schematic illustration of future efforts in studying high-voltage behavior of SIB cathodes using synchrotron X-ray and neutron scattering technology.

1. Investigating CEI in high-voltage polyanion-type cathode: Investigations into the CEI of polyanion-type cathode materials have attracted substantial interest. However, most of the reported results in this area are from lab-based characterizations, which suggests that there is plenty of scope for applying synchrotron X-ray and neutron scattering techniques. As a successful example, the use of synchrotron-based soft XAS with both FY and TEY mode was able to reveal the transition metal activity in the CEI of layered transition metal oxide cathodes. More similar advanced techniques are encouraged for application in the investigation of the CEI of high-voltage polyanion-type cathodes to obtain more insights with the hope of extending cell lifetime;
2. Extending neutron scattering techniques: In the research area of high-voltage SIB cathode materials, ND has been widely used to study the bulk structure of layered

transition metal oxide cathodes and polyanion-type cathodes. There remains wide scope for using neutron scattering techniques in CEI studies. SANS is a powerful tool for obtaining the size and shape information of materials at the nanometer scale which has been successfully used in studying the chemical nature, morphology, and size evolution of the solid–electrolyte interphase (SEI) in LIBs [117,118]. Neutron reflection testing is able to probe the structure and kinetics at the materials' interphase by detecting the reflected intensity as a function of angle, which has been used to study the structure and composition gradients of SEI in LIBs [119,120]. These successful examples from LIBs suggest the possibility of involving these neutron-scattering-based techniques in SIB CEI studies from different perspectives;

3. Exploring new techniques: To accelerate the understanding of the SIB cathode's behavior at high voltage, more synchrotron-X-ray- and neutron-based complementary techniques are needed to obtain a more complete picture of the material's structure, dynamics, and electrochemical behavior. For example, the introduction of dark-field X-ray microscopy [121] could complement TXM in characterizing material morphology by enhancing contrast with selective detection of scattered X-rays. Especially, dark-field X-ray microscopy [121] is highly sensitive to surface features, which could provide valuable information about the interphase morphology. Due to the sensitivity to the dynamic behavior of nanoscale features, the use of X-ray photon correlation spectroscopy (XPCS) could provide information about the movement and fluctuations of nanoparticles and crystal domains [122,123]. This is important for understanding working ion diffusion, phase transitions, and structural heterogeneities or defects on the nanosecond to microsecond timescales;
4. Bridging materials characterizations to electrode performance: Although there have been substantial efforts towards understanding high-voltage SIB cathode materials using synchrotron X-ray and neutron scattering techniques, it is challenging to directly link the materials characterization results with the electrode, as well as cell device performance partially due to the disconnection between morphology and phase characterization. One finds it is difficult to perform transmission microscopy and diffraction for the same batch of particles to obtain morphology and phase change information simultaneously. It would be ideal if we could collect morphology and structural phase information for a controllable number of particles at the same time in the near future. By studying the behavior of these particles statistically, one could establish a model to predict the electrode performance with the aid of artificial intelligence, which could also guide the selection of the materials synthesis methodology.

Author Contributions: Conceptualization, B.S. and L.M.; writing—original draft preparation, V.S., R.J. and L.M.; writing—review and editing, W.Z., B.S. and L.M.; funding acquisition, L.M. All authors have read and agreed to the published version of the manuscript.

Funding: This research was funded by [the US National Science Foundation] grant number [2301719].

Acknowledgments: Lin Ma at UNC Charlotte acknowledges the support by the US National Science Foundation, award no. 2301719.

Conflicts of Interest: The authors declare no conflict of interest.

References

1. Wang, W.; Yuan, B.; Sun, Q.; Wennersten, R. Application of Energy Storage in Integrated Energy Systems—A Solution to Fluctuation and Uncertainty of Renewable Energy. *J. Energy Storage* **2022**, *52*, 104812. [CrossRef]
2. Kebede, A.A.; Kalogiannis, T.; Van Mierlo, J.; Berecibar, M. A Comprehensive Review of Stationary Energy Storage Devices for Large Scale Renewable Energy Sources Grid Integration. *Renew. Sustain. Energy Rev.* **2022**, *159*, 112213. [CrossRef]
3. Xu, J. Critical Review on Cathode–Electrolyte Interphase toward High-Voltage Cathodes for Li-Ion Batteries. *Nano-Micro Lett.* **2022**, *14*, 166. [CrossRef]
4. Xu, J.; Zhang, J.; Pollard, T.P.; Li, Q.; Tan, S.; Hou, S.; Wan, H.; Chen, F.; He, H.; Hu, E.; et al. Electrolyte Design for Li-Ion Batteries under Extreme Operating Conditions. *Nature* **2023**, *614*, 694–700. [CrossRef]
5. Ray, A.; Saruhan, B. Application of Ionic Liquids for Batteries and Supercapacitors. *Materials* **2021**, *14*, 2942. [CrossRef] [PubMed]

6. Li, H.; Cormier, M.; Zhang, N.; Inglis, J.; Li, J.; Dahn, J.R. Is Cobalt Needed in Ni-Rich Positive Electrode Materials for Lithium Ion Batteries? *J. Electrochem. Soc.* **2019**, *166*, A429. [CrossRef]
7. Zhang, N.; Zaker, N.; Li, H.; Liu, A.; Inglis, J.; Jing, L.; Li, J.; Li, Y.; Botton, G.A.; Dahn, J.R. Cobalt-Free Nickel-Rich Positive Electrode Materials with a Core–Shell Structure. *Chem. Mater.* **2019**, *31*, 10150–10160. [CrossRef]
8. Hwang, J.-Y.; Myung, S.-T.; Sun, Y.-K. Sodium-Ion Batteries: Present and Future. *Chem. Soc. Rev.* **2017**, *46*, 3529–3614. [CrossRef] [PubMed]
9. Li, M.; Du, Z.; Khaleel, M.A.; Belharouak, I. Materials and Engineering Endeavors Towards Practical Sodium-Ion Batteries. *Energy Storage Mater.* **2020**, *25*, 520–536. [CrossRef]
10. Fang, C.; Huang, Y.; Zhang, W.; Han, J.; Deng, Z.; Cao, Y.; Yang, H. Routes to High Energy Cathodes of Sodium-Ion Batteries. *Adv. Energy Mater.* **2016**, *6*, 1501727. [CrossRef]
11. Lei, Z.-Q.; Guo, Y.-J.; Wang, E.-H.; He, W.-H.; Zhang, Y.-Y.; Xin, S.; Yin, Y.-X.; Guo, Y.-G. Layered Oxide Cathode-Electrolyte Interface Towards Na-Ion Batteries: Advances and Perspectives. *Chem. Asian J.* **2022**, *17*, e202200213. [CrossRef] [PubMed]
12. Boivin, E.; House, R.A.; Marie, J.-J.; Bruce, P.G. Controlling Iron Versus Oxygen Redox in the Layered Cathode Na0.67fe0.5mn0.5o2: Mitigating Voltage and Capacity Fade by Mg Substitution. *Adv. Energy Mater.* **2022**, *12*, 2200702. [CrossRef]
13. Clément, R.J.; Bruce, P.G.; Grey, C.P. Review—Manganese-Based P2-Type Transition Metal Oxides as Sodium-Ion Battery Cathode Materials. *J. Electrochem. Soc.* **2015**, *162*, A2589. [CrossRef]
14. Li, Z.; Kong, W.; Yu, Y.; Zhang, J.; Wong, D.; Xu, Z.; Chen, Z.; Schulz, C.; Bartkowiak, M.; Liu, X. Tuning Bulk O_2 and Nonbonding Oxygen State for Reversible Anionic Redox Chemistry in P2-Layered Cathodes. *Angew. Chem. Int. Ed.* **2022**, *61*, e202115552. [CrossRef] [PubMed]
15. Liu, H.; Gao, X.; Chen, J.; Gao, J.; Yin, S.; Zhang, S.; Ji, X. Reversible OP4 Phase in P2–$Na_{2/3}Ni_{1/3}Mn_{2/3}O_2$ Sodium Ion Cathode. *J. Power Sources* **2021**, *508*, 230324. [CrossRef]
16. Liu, J.; Didier, C.; Sale, M.; Sharma, N.; Guo, Z.; Peterson, V.K.; Ling, C.D. Elucidation of the High-Voltage Phase in the Layered Sodium Ion Battery Cathode Material P3–$Na_{0.5}Ni_{0.25}Mn_{0.75}O_2$. *J. Mater. Chem. A* **2020**, *8*, 21151–21162. [CrossRef]
17. Wu, H.; Chen, Y.; Wen, T.; Chen, L.; Pu, X.; Chen, Z. Advances in Vanadium-Redoxed Polyanions for High-Voltage Sodium-Ion Batteries. *Batteries* **2023**, *9*, 56. [CrossRef]
18. Subramanian, Y.; Oh, W.; Choi, W.; Lee, H.; Jeong, M.; Thangavel, R.; Yoon, W.-S. Optimizing High Voltage $Na_3V_2(PO_4)_2F_3$ Cathode for Achieving High Rate Sodium-Ion Batteries with Long Cycle Life. *Chem. Eng. J.* **2021**, *403*, 126291. [CrossRef]
19. Berlanga, C.; Monterrubio, I.; Armand, M.; Rojo, T.; Galceran, M.; Casas-Cabanas, M. Cost-Effective Synthesis of Triphylite-$NaFePO_4$ Cathode: A Zero-Waste Process. *ACS Sustain. Chem. Eng.* **2020**, *8*, 725–730. [CrossRef]
20. Tang, W.; Song, X.; Du, Y.; Peng, C.; Lin, M.; Xi, S.; Tian, B.; Zheng, J.; Wu, Y.; Pan, F.; et al. High-Performance $NaFePO_4$ Formed by Aqueous Ion-Exchange and Its Mechanism for Advanced Sodium Ion Batteries. *J. Mater. Chem. A* **2016**, *4*, 4882–4892. [CrossRef]
21. Dong, J.; Xiao, J.; Yu, Y.; Wang, J.; Chen, F.; Wang, S.; Zhang, L.; Ren, N.; Pan, B.; Chen, C. Electronic Structure Regulation of Na_2FePO_4F Cathode toward Superior High-Rate and High-Temperature Sodium-Ion Batteries. *Energy Storage Mater.* **2022**, *45*, 851–860. [CrossRef]
22. Li, H.; Wang, T.; Wang, S.; Wang, X.; Xie, Y.; Hu, J.; Lai, Y.; Zhang, Z. Scalable Synthesis of the Na_2FePO_4F Cathode through an Economical and Reliable Approach for Sodium-Ion Batteries. *ACS Sustain. Chem. Eng.* **2021**, *9*, 11798–11806. [CrossRef]
23. Barpanda, P.; Liu, G.; Ling, C.D.; Tamaru, M.; Avdeev, M.; Chung, S.-C.; Yamada, Y.; Yamada, A. $Na_2FeP_2O_7$: A Safe Cathode for Rechargeable Sodium-Ion Batteries. *Chem. Mater.* **2013**, *25*, 3480–3487. [CrossRef]
24. Jung, Y.H.; Lim, C.H.; Kim, J.-H.; Kim, D.K. $Na_2FeP_2O_7$ as a Positive Electrode Material for Rechargeable Aqueous Sodium-Ion Batteries. *RSC Adv.* **2014**, *4*, 9799–9802. [CrossRef]
25. Plewa, A.; Kulka, A.; Baster, D.; Molenda, J. An Alluaudite Compounds $Na_2Fe_2(SO_4)_3$ Vs. $Na_{2.5}Fe_{1.75}(SO_4)_3$ as Earth Abundant Cathode Materials for Na-Ion Batteries. *Solid State Ion.* **2019**, *335*, 15–22. [CrossRef]
26. Shishkin, M.; Sato, H. Ab Initio Study of Stability of $Na_2Fe_2(SO_4)_3$, a High Potential Na-Ion Battery Cathode Material. *J. Phys. Chem. C* **2017**, *121*, 20067–20074. [CrossRef]
27. Liu, Y.; Qiao, Y.; Zhang, W.; Li, Z.; Ji, X.; Miao, L.; Yuan, L.; Hu, X.; Huang, Y. Sodium Storage in Na-Rich $Na_xFeFe(CN)_6$ Nanocubes. *Nano Energy* **2015**, *12*, 386–393. [CrossRef]
28. Wang, Y.P.; Hou, B.P.; Cao, X.R.; Wu, S.Q.; Zhu, Z.Z. Structural Evolution, Redox Mechanism, and Ionic Diffusion in Rhombohedral $Na_2FeFe(CN)_6$ for Sodium-Ion Batteries: First-Principles Calculations. *J. Electrochem. Soc.* **2022**, *169*, 010525. [CrossRef]
29. Xiao, P.; Song, J.; Wang, L.; Goodenough, J.B.; Henkelman, G. Theoretical Study of the Structural Evolution of a $Na_2FeMn(CN)_6$ Cathode Upon Na Intercalation. *Chem. Mater.* **2015**, *27*, 3763–3768. [CrossRef]
30. Liu, Z.; Zhang, W.; Jiang, Y. Synthesis of $Na_2Mn_{0.8}Fe_{0.2}Fe(CN)_6$ and Its Application as Cathode Material of Sodium Ion Battery. *IOP Conf. Ser. Earth Environ. Sci.* **2021**, *621*, 012061. [CrossRef]
31. Ma, X.-H.; Wei, Y.-Y.; Wu, Y.-D.; Wang, J.; Jia, W.; Zhou, J.-H.; Zi, Z.-F.; Dai, J.-M. High Crystalline $Na_2Ni[Fe(CN)_6]$ Particles for a High-Stability and Low-Temperature Sodium-Ion Batteries Cathode. *Electrochim. Acta* **2019**, *297*, 392–397. [CrossRef]
32. Su, X.; Wang, Y.; Zhou, J.; Gu, S.; Li, J.; Zhang, S. Operando Spectroscopic Identification of Active Sites in NiFe Prussian Blue Analogues as Electrocatalysts: Activation of Oxygen Atoms for Oxygen Evolution Reaction. *J. Am. Chem. Soc.* **2018**, *140*, 11286–11292. [CrossRef] [PubMed]

33. Zhang, H.; Gao, Y.; Liu, X.; Yang, Z.; He, X.; Li, L.; Qiao, Y.; Chen, W.; Zeng, R.; Wang, Y.; et al. Organic Cathode Materials for Sodium-Ion Batteries: From Fundamental Research to Potential Commercial Application. *Adv. Funct. Mater.* **2022**, *32*, 2107718. [CrossRef]
34. Delmas, C.; Fouassier, C.; Hagenmuller, P. Structural Classification and Properties of the Layered Oxides. *Phys. B Phys. C* **1980**, *99*, 81–85. [CrossRef]
35. Peng, B.; Sun, Z.; Jiao, S.; Wang, G.; Zhang, G. Electrochemical Performance Optimization of Layered P2-Type $Na_{0.67}MnO_2$ through Simultaneous Mn-Site Doping and Nanostructure Engineering. *Batter. Supercaps* **2020**, *3*, 147–154. [CrossRef]
36. Guo, J.-Z.; Gu, Z.-Y.; Du, M.; Zhao, X.-X.; Wang, X.-T.; Wu, X.-L. Emerging Characterization Techniques for Delving Polyanion-Type Cathode Materials of Sodium-Ion Batteries. *Mater. Today* **2023**, *66*, 221–244. [CrossRef]
37. You, Y.; Manthiram, A. Progress in High-Voltage Cathode Materials for Rechargeable Sodium-Ion Batteries. *Adv. Energy Mater.* **2018**, *8*, 1701785. [CrossRef]
38. Peng, J.; Zhang, W.; Liu, Q.; Wang, J.; Chou, S.; Liu, H.; Dou, S. Prussian Blue Analogues for Sodium-Ion Batteries: Past, Present, and Future. *Adv. Mater.* **2022**, *34*, 2108384. [CrossRef]
39. Rajagopalan, R.; Tang, Y.; Jia, C.; Ji, X.; Wang, H. Understanding the Sodium Storage Mechanisms of Organic Electrodes in Sodium Ion Batteries: Issues and Solutions. *Energy Environ. Sci.* **2020**, *13*, 1568–1592. [CrossRef]
40. Xiang, X.; Zhang, K.; Chen, J. Recent Advances and Prospects of Cathode Materials for Sodium-Ion Batteries. *Adv. Mater.* **2015**, *27*, 5343–5364. [CrossRef]
41. Xiao, J.; Li, X.; Tang, K.; Wang, D.; Long, M.; Gao, H.; Chen, W.; Liu, C.; Liu, H.; Wang, G. Recent Progress of Emerging Cathode Materials for Sodium Ion Batteries. *Mater. Chem. Front.* **2021**, *5*, 3735–3764. [CrossRef]
42. Lin, F.; Liu, Y.; Yu, X.; Cheng, L.; Singer, A.; Shpyrko, O.G.; Xin, H.L.; Tamura, N.; Tian, C.; Weng, T.-C.; et al. Synchrotron X-Ray Analytical Techniques for Studying Materials Electrochemistry in Rechargeable Batteries. *Chem. Rev.* **2017**, *117*, 13123–13186. [CrossRef] [PubMed]
43. Chen, M.; Chou, S.-L.; Dou, S.-X. Understanding Challenges of Cathode Materials for Sodium-Ion Batteries Using Synchrotron-Based X-Ray Absorption Spectroscopy. *Batter. Supercaps* **2019**, *2*, 842–851. [CrossRef]
44. Gu, Q.; Kimpton, J.A.; Brand, H.E.A.; Wang, Z.; Chou, S. Solving Key Challenges in Battery Research Using in Situ Synchrotron and Neutron Techniques. *Adv. Energy Mater.* **2017**, *7*, 1602831. [CrossRef]
45. Zhao, C.; Lu, Y.; Li, Y.; Jiang, L.; Rong, X.; Hu, Y.-S.; Li, H.; Chen, L. Novel Methods for Sodium-Ion Battery Materials. *Small Methods* **2017**, *1*, 1600063. [CrossRef]
46. Shah, A.R.; Shutt, R.R.C.; Smith, K.; Hack, J.; Neville, T.P.; Headen, T.F.; Brett, D.J.L.; Howard, C.A.; Miller, T.S.; Cullen, P.L. Neutron Studies of Na-Ion Battery Materials. *J. Phys. Mater.* **2021**, *4*, 042008. [CrossRef]
47. Pérez, G.E.; Brittain, J.M.; McClelland, I.; Hull, S.; Jones, M.O.; Playford, H.Y.; Cussen, S.A.; Baker, P.J.; Reynolds, E.M. Neutron and Muon Characterisation Techniques for Battery Materials. *J. Mater. Chem. A* **2023**, *11*, 10493–10531. [CrossRef]
48. Zhao, E.; Wang, H.; Yin, W.; He, L.; Ke, Y.; Wang, F.; Zhao, J. Spatiotemporal-Scale Neutron Studies on Lithium-Ion Batteries and Beyond. *Appl. Phys. Lett.* **2022**, *121*, 110501. [CrossRef]
49. Ren, Y.; Zuo, X. Synchrotron X-Ray and Neutron Diffraction, Total Scattering, and Small-Angle Scattering Techniques for Rechargeable Battery Research. *Small Methods* **2018**, *2*, 1800064. [CrossRef]
50. Delmas, C.; Braconnier, J.-J.; Fouassier, C.; Hagenmuller, P. Electrochemical Intercalation of Sodium in Na_xCoO_2 Bronzes. *Solid State Ion.* **1981**, *3-4*, 165–169. [CrossRef]
51. Gupta, P.; Pushpakanth, S.; Haider, M.A.; Basu, S. Understanding the Design of Cathode Materials for Na-Ion Batteries. *ACS Omega* **2022**, *7*, 5605–5614. [CrossRef] [PubMed]
52. Liu, J.; Kan, W.H.; Ling, C.D. Insights into the High Voltage Layered Oxide Cathode Materials in Sodium-Ion Batteries: Structural Evolution and Anion Redox. *J. Power Sources* **2021**, *481*, 229139. [CrossRef]
53. Kang, W.; Yu, D.Y.W.; Lee, P.-K.; Zhang, Z.; Bian, H.; Li, W.; Ng, T.-W.; Zhang, W.; Lee, C.-S. P2-Type $Na_xCu_{0.15}Ni_{0.20}Mn_{0.65}O_2$ Cathodes with High Voltage for High-Power and Long-Life Sodium-Ion Batteries. *ACS Appl. Mater. Interfaces* **2016**, *8*, 31661–31668. [CrossRef]
54. Wu, X.; Guo, J.; Wang, D.; Zhong, G.; McDonald, M.J.; Yang, Y. P2-Type $Na_{0.66}Ni_{0.33}$–$XZn_xMn_{0.67}O_2$ as New High-Voltage Cathode Materials for Sodium-Ion Batteries. *J. Power Sources* **2015**, *281*, 18–26. [CrossRef]
55. Xu, G.-L.; Amine, R.; Xu, Y.-F.; Liu, J.; Gim, J.; Ma, T.; Ren, Y.; Sun, C.-J.; Liu, Y.; Zhang, X.; et al. Insights into the Structural Effects of Layered Cathode Materials for High Voltage Sodium-Ion Batteries. *Energy Environ. Sci.* **2017**, *10*, 1677–1693. [CrossRef]
56. Wang, K.; Wan, H.; Yan, P.; Chen, X.; Fu, J.; Liu, Z.; Deng, H.; Gao, F.; Sui, M. Dopant Segregation Boosting High-Voltage Cyclability of Layered Cathode for Sodium Ion Batteries. *Adv. Mater.* **2019**, *31*, 1904816. [CrossRef]
57. Konarov, A.; Kim, H.J.; Jo, J.-H.; Voronina, N.; Lee, Y.; Bakenov, Z.; Kim, J.; Myung, S.-T. High-Voltage Oxygen-Redox-Based Cathode for Rechargeable Sodium-Ion Batteries. *Adv. Energy Mater.* **2020**, *10*, 2001111. [CrossRef]
58. Matsui, M.; Mizukoshi, F.; Hasegawa, H.; Imanishi, N. Ca-Substituted P3-Type $Na_xNi_{1/3}Mn_{1/3}Co_{1/3}O_2$ as a Potential High Voltage Cathode Active Material for Sodium-Ion Batteries. *J. Power Sources* **2021**, *485*, 229346. [CrossRef]
59. Jiang, K.; Zhang, X.; Li, H.; Zhang, X.; He, P.; Guo, S.; Zhou, H. Suppressed the High-Voltage Phase Transition of P2-Type Oxide Cathode for High-Performance Sodium-Ion Batteries. *ACS Appl. Mater. Interfaces* **2019**, *11*, 14848–14853. [CrossRef]
60. Pei, Q.; Lu, M.; Liu, Z.; Li, D.; Rao, X.; Liu, X.; Zhong, S. Improving the $Na_{0.67}Ni_{0.33}Mn_{0.67}O_2$ Cathode Material for High-Voltage Cyclability Via Ti/Cu Codoping for Sodium-Ion Batteries. *ACS Appl. Energy Mater.* **2022**, *5*, 1953–1962. [CrossRef]

61. Bhange, D.S.; Ali, G.; Kim, D.-H.; Anang, D.A.; Shin, T.J.; Kim, M.-G.; Kang, Y.-M.; Chung, K.Y.; Nam, K.-W. Honeycomb-Layer Structured $Na_3Ni_2BiO_6$ as a High Voltage and Long Life Cathode Material for Sodium-Ion Batteries. *J. Mater. Chem. A* **2017**, *5*, 1300–1310. [CrossRef]
62. Tapia-Ruiz, N.; Dose, W.M.; Sharma, N.; Chen, H.; Heath, J.; Somerville, J.W.; Maitra, U.; Islam, M.S.; Bruce, P.G. High Voltage Structural Evolution and Enhanced Na-Ion Diffusion in P2-$Na_{2/3}Ni_{1/3}-XMg_xMn_{2/3}O_2$ ($0 \leq X \leq 0.2$) Cathodes from Diffraction, Electrochemical and Ab Initio Studies. *Energy Environ. Sci.* **2018**, *11*, 1470–1479. [CrossRef]
63. Wang, L.; Wang, J.; Zhang, X.; Ren, Y.; Zuo, P.; Yin, G.; Wang, J. Unravelling the Origin of Irreversible Capacity Loss in $NaNiO_2$ for High Voltage Sodium Ion Batteries. *Nano Energy* **2017**, *34*, 215–223. [CrossRef]
64. Jeong, M.; Lee, H.; Yoon, J.; Yoon, W.-S. O3-Type $NaNi_{1/3}Fe_{1/3}Mn_{1/3}O_2$ Layered Cathode for Na-Ion Batteries: Structural Evolution and Redox Mechanism Upon Na (De) Intercalation. *J. Power Sources* **2019**, *439*, 227064. [CrossRef]
65. Huang, Y.; Yan, Z.; Luo, W.; Hu, Z.; Liu, G.; Zhang, L.; Huang, Y. Vitalization of P2–$Na_{2/3}Ni_{1/3}Mn_{2/3}O_2$ at High-Voltage Cyclability Via Combined Structural Modulation for Sodium-Ion Batteries. *Energy Storage Mater.* **2020**, *29*, 182–189. [CrossRef]
66. Xu, J.; Lee, D.H.; Clément, R.J.; Yu, X.; Leskes, M.; Pell, A.J.; Pintacuda, G.; Yang, X.-Q.; Grey, C.P.; Meng, Y.S. Identifying the Critical Role of Li Substitution in P2–$Na_x[Li_yNi_zMn_{1-Y-Z}]O_2$ ($0 < X, Y, Z < 1$) Intercalation Cathode Materials for High-Energy Na-Ion Batteries. *Chem. Mater.* **2014**, *26*, 1260–1269.
67. Liu, K.; Tan, S.; Moon, J.; Jafta, C.J.; Li, C.; Kobayashi, T.; Dai, S. Insights into the Enhanced Cycle and Rate Performances of the F-Substituted P2-Type Oxide Cathodes for Sodium-Ion Batteries. *Adv. Energy Mater.* **2020**, *10*, 2000135. [CrossRef]
68. Clément, R.J.; Billaud, J.; Robert Armstrong, A.; Singh, G.; Rojo, T.; Bruce, P.G.; Grey, C.P. Structurally Stable Mg-Doped P2-$Na_{2/3}Mn_{1-Y}Mg_yO_2$ Sodium-Ion Battery Cathodes with High Rate Performance: Insights from Electrochemical, NMR and Diffraction Studies. *Energy Environ. Sci.* **2016**, *9*, 3240–3251. [CrossRef]
69. Zhou, D.; Ning, D.; Wang, J.; Liu, J.; Zhang, G.; Xiao, Y.; Zheng, J.; Li, Y.; Li, J.; Liu, X. Clarification of Underneath Capacity Loss for O3-Type Ni, Co Free Layered Cathodes at High Voltage for Sodium Ion Batteries. *J. Energy Chem.* **2023**, *77*, 479–486. [CrossRef]
70. Park, J.-H.; Ko, I.-H.; Lee, J.; Park, S.; Kim, D.; Yu, S.-H.; Sung, Y.-E. Anionic Redox Reactions in Cathodes for Sodium-Ion Batteries. *ChemElectroChem* **2021**, *8*, 625–643. [CrossRef]
71. Voronina, N.; Shin, M.Y.; Kim, H.J.; Yaqoob, N.; Guillon, O.; Song, S.H.; Myung, S.T. Hysteresis-Suppressed Reversible Oxygen-Redox Cathodes for Sodium-Ion Batteries. *Adv. Energy Mater.* **2022**, *12*, 2103939. [CrossRef]
72. Yu, Y.; Ning, D.; Li, Q.; Franz, A.; Zheng, L.; Zhang, N.; Ren, G.; Schumacher, G.; Liu, X. Revealing the Anionic Redox Chemistry in O3-Type Layered Oxide Cathode for Sodium-Ion Batteries. *Energy Storage Mater.* **2021**, *38*, 130–140. [CrossRef]
73. Ji, H.; Ji, W.; Xue, H.; Chen, G.; Qi, R.; Huang, Z.; Fang, H.; Chu, M.; Liu, L.; Ma, Z.; et al. Synergistic Activation of Anionic Redox Via Cosubstitution to Construct High-Capacity Layered Oxide Cathode Materials for Sodium-Ion Batteries. *Sci. Bull.* **2023**, *68*, 65–76. [CrossRef] [PubMed]
74. Song, B.; Hu, E.; Liu, J.; Zhang, Y.; Yang, X.-Q.; Nanda, J.; Huq, A.; Page, K. A Novel P3-Type $Na_{2/3}Mg_{1/3}Mn_{2/3}O_2$ as High Capacity Sodium-Ion Cathode Using Reversible Oxygen Redox. *J. Mater. Chem. A* **2019**, *7*, 1491–1498. [CrossRef]
75. Rong, X.; Liu, J.; Hu, E.; Liu, Y.; Wang, Y.; Wu, J.; Yu, X.; Page, K.; Hu, Y.-S.; Yang, W.; et al. Structure-Induced Reversible Anionic Redox Activity in Na Layered Oxide Cathode. *Joule* **2018**, *2*, 125–140. [CrossRef]
76. House, R.A.; Maitra, U.; Pérez-Osorio, M.A.; Lozano, J.G.; Jin, L.; Somerville, J.W.; Duda, L.C.; Nag, A.; Walters, A.; Zhou, K.-J.; et al. Superstructure Control of First-Cycle Voltage Hysteresis in Oxygen-Redox Cathodes. *Nature* **2020**, *577*, 502–508. [CrossRef]
77. Mu, L.; Feng, X.; Kou, R.; Zhang, Y.; Guo, H.; Tian, C.; Sun, C.; Du, X.; Nordlund, D.; Xin, H.L.; et al. Deciphering the Cathode–Electrolyte Interfacial Chemistry in Sodium Layered Cathode Materials. *Adv. Energy Mater.* **2018**, *8*, 1801975. [CrossRef]
78. Song, J.; Xiao, B.; Lin, Y.; Xu, K.; Li, X. Interphases in Sodium-Ion Batteries. *Adv. Energy Mater.* **2018**, *8*, 1703082. [CrossRef]
79. Xu, K. Electrolytes and Interphases in Li-Ion Batteries and Beyond. *Chem. Rev.* **2014**, *114*, 11503–11618. [CrossRef]
80. Lin, F.; Nordlund, D.; Markus, I.M.; Weng, T.-C.; Xin, H.L.; Doeff, M.M. Profiling the Nanoscale Gradient in Stoichiometric Layered Cathode Particles for Lithium-Ion Batteries. *Energy Environ. Sci.* **2014**, *7*, 3077–3085. [CrossRef]
81. Mu, L.; Rahman, M.M.; Zhang, Y.; Feng, X.; Du, X.-W.; Nordlund, D.; Lin, F. Surface Transformation by a "Cocktail" Solvent Enables Stable Cathode Materials for Sodium Ion Batteries. *J. Mater. Chem. A* **2018**, *6*, 2758–2766. [CrossRef]
82. Doubaji, S.; Philippe, B.; Saadoune, I.; Gorgoi, M.; Gustafsson, T.; Solhy, A.; Valvo, M.; Rensmo, H.; Edström, K. Passivation Layer and Cathodic Redox Reactions in Sodium-Ion Batteries Probed by Haxpes. *ChemSusChem* **2016**, *9*, 97–108. [CrossRef] [PubMed]
83. Rahman, M.M.; Xu, Y.; Cheng, H.; Shi, Q.; Kou, R.; Mu, L.; Liu, Q.; Xia, S.; Xiao, X.; Sun, C.-J.; et al. Empowering Multicomponent Cathode Materials for Sodium Ion Batteries by Exploring Three-Dimensional Compositional Heterogeneities. *Energy Environ. Sci.* **2018**, *11*, 2496–2508. [CrossRef]
84. Pan, J.; Zhang, Y.; Sun, F.; Osenberg, M.; Hilger, A.; Manke, I.; Cao, R.; Dou, S.X.; Fan, H.J. Designing Solvated Double-Layer Polymer Electrolytes with Molecular Interactions Mediated Stable Interfaces for Sodium Ion Batteries. *Angew. Chem. Int. Ed.* **2023**, *62*, e202219000. [CrossRef]
85. Manthiram, A.; Goodenough, J.B. Lithium Insertion into $Fe_2(SO_4)_3$ Frameworks. *J. Power Sources* **1989**, *26*, 403–408. [CrossRef]
86. Fang, Y.; Liu, Q.; Xiao, L.; Rong, Y.; Liu, Y.; Chen, Z.; Ai, X.; Cao, Y.; Yang, H.; Xie, J.; et al. A Fully Sodiated Navopo4 with Layered Structure for High-Voltage and Long-Lifespan Sodium-Ion Batteries. *Chem* **2018**, *4*, 1167–1180. [CrossRef]
87. Deng, L.; Yu, F.-D.; Xia, Y.; Jiang, Y.-S.; Sui, X.-L.; Zhao, L.; Meng, X.-H.; Que, L.-F.; Wang, Z.-B. Stabilizing Fluorine to Achieve High-Voltage and Ultra-Stable $Na_3V_2(PO_4)_2F_3$ Cathode for Sodium Ion Batteries. *Nano Energy* **2021**, *82*, 105659. [CrossRef]

88. Song, T.; Yao, W.; Kiadkhunthod, P.; Zheng, Y.; Wu, N.; Zhou, X.; Tunmee, S.; Sattayaporn, S.; Tang, Y. A Low-Cost and Environmentally Friendly Mixed Polyanionic Cathode for Sodium-Ion Storage. *Angew. Chem. Int. Ed.* **2020**, *59*, 740–745. [CrossRef]
89. Wang, J.; Zeng, W.; Zhu, J.; Xia, F.; Zhao, H.; Tian, W.; Wang, T.; Zhang, Y.; Zhang, S.; Mu, S. Fe-Rich Pyrophosphate with Prolonged High-Voltage-Plateaus and Suppressed Voltage Decay as Sodium-Ion Battery Cathode. *Nano Energy* **2023**, *116*, 108822. [CrossRef]
90. Tong, S.; Pan, H.; Liu, H.; Zhang, X.; Liu, X.; Jia, M.; Kang, Y.; Yuan, Y.; Du, X.; Yan, X. Titanium Doping Induced the Suppression of Irreversible Phase Transformation at High Voltage for V-Based Phosphate Cathodes of Na-Ion Batteries. *ChemSusChem* **2023**, *16*, e202300244. [CrossRef]
91. Gao, H.; Seymour, I.D.; Xin, S.; Xue, L.; Henkelman, G.; Goodenough, J.B. $Na_3MnZr(PO_4)_3$: A High-Voltage Cathode for Sodium Batteries. *J. Am. Chem. Soc.* **2018**, *140*, 18192–18199. [CrossRef] [PubMed]
92. Zhang, W.; Li, H.; Zhang, Z.; Xu, M.; Lai, Y.; Chou, S.-L. Full Activation of Mn^{4+}/Mn^{3+} Redox in $Na_4MnCr(PO_4)_3$ as a High-Voltage and High-Rate Cathode Material for Sodium-Ion Batteries. *Small* **2020**, *16*, 2001524. [CrossRef] [PubMed]
93. Chen, M.; Hua, W.; Xiao, J.; Cortie, D.; Guo, X.; Wang, E.; Dou, S.X. Development and Investigation of a Nasicon-Type High-Voltage Cathode Material for High-Power Sodium-Ion Batteries. *Angew. Chem. Int. Ed.* **2020**, *59*, 2449–2456. [CrossRef] [PubMed]
94. Wang, J.; Wang, Y.; Seo, D.-H.; Shi, T.; Chen, S.; Tian, Y.; Kim, H.; Ceder, G. A High-Energy Nasicon-Type Cathode Material for Na-Ion Batteries. *Adv. Energy Mater.* **2020**, *10*, 1903968. [CrossRef]
95. Nishimura, S.-I.; Suzuki, Y.; Lu, J.; Torii, S.; Kamiyama, T.; Yamada, A. High-Temperature Neutron and X-Ray Diffraction Study of Fast Sodium Transport in Alluaudite-Type Sodium Iron Sulfate. *Chem. Mater.* **2016**, *28*, 2393–2399. [CrossRef]
96. Zhang, J.; Liu, Y.; Zhao, X.; He, L.; Liu, H.; Song, Y.; Sun, S.; Li, Q.; Xing, X.; Chen, J. A Novel Nasicon-Type $Na_4MnCr(PO_4)_3$ Demonstrating the Energy Density Record of Phosphate Cathodes for Sodium-Ion Batteries. *Adv. Mater.* **2020**, *32*, 1906348. [CrossRef]
97. Buryak, N.S.; Anishchenko, D.V.; Levin, E.E.; Ryazantsev, S.V.; Martin-Diaconescu, V.; Zakharkin, M.V.; Nikitina, V.A.; Antipov, E.V. High-Voltage Structural Evolution and Its Kinetic Consequences for the $Na_4MnV(PO_4)_3$ Sodium-Ion Battery Cathode Material. *J. Power Sources* **2022**, *518*, 230769. [CrossRef]
98. Kawai, K.; Zhao, W.; Nishimura, S.-I.; Yamada, A. High-Voltage Cr^{4+}/Cr^{3+} Redox Couple in Polyanion Compounds. *ACS Appl. Energy Mater.* **2018**, *1*, 928–931. [CrossRef]
99. Qin, B.; Zarrabeitia, M.; Hoefling, A.; Jusys, Z.; Liu, X.; Tübke, J.; Behm, R.J.; Cui, G.; Varzi, A.; Passerini, S. A Unique Polymer-Inorganic Cathode-Electrolyte-Interphase (Cei) Boosts High-Performance $Na_3V_2(PO_4)_2F_3$ Batteries in Ether Electrolytes. *J. Power Sources* **2023**, *560*, 232630. [CrossRef]
100. He, J.; Tao, T.; Yang, F.; Sun, Z. Optimizing the Electrolyte Systems for $Na_3(VO_{1-X}PO_4)2F_{1+2x}$ ($0 \leq X \leq 1$) Cathode and Understanding Their Interfacial Chemistries Towards High-Rate Sodium-Ion Batteries. *ChemSusChem* **2022**, *15*, e202102522. [CrossRef]
101. He, J.; Tao, T.; Yang, F.; Sun, Z. Unravelling Li+ Intercalation Mechanism and Cathode Electrolyte Interphase of $Na_3V_2(PO_4)_3$ and $Na_3(VOPO_4)2F$ Cathode as Robust Framework Towards High-Performance Lithium-Ion Batteries. *ChemSusChem* **2022**, *15*, e202200817. [CrossRef] [PubMed]
102. Zhang, Y.; Zhang, J.; Shao, T.; Li, X.; Chen, G.; Liu, H.; Ma, Z.-F. Mg2+-Doping Constructed a Continuous and Homogeneous Cathode-Electrolyte Interphase Film on $Na_{3.12}Fe_{2.44}(P_2O_7)_2$ with Superior and Stable High-Temperature Performance for Sodium-Ion Storage. *ACS Appl. Mater. Interfaces* **2022**, *14*, 14253–14263. [CrossRef]
103. Ihsan-Ul-Haq, M.; Cui, J.; Mubarak, N.; Xu, M.; Shen, X.; Luo, Z.; Huang, B.; Kim, J.-K. Revealing Cathode–Electrolyte Interface on Flower-Shaped $Na_3V_2(PO_4)_3/C$ Cathode through Cryogenic Electron Microscopy. *Adv. Energy Sustain. Res.* **2021**, *2*, 2100072. [CrossRef]
104. Lee, Y.; Lee, J.; Kim, H.; Kang, K.; Choi, N.-S. Highly Stable Linear Carbonate-Containing Electrolytes with Fluoroethylene Carbonate for High-Performance Cathodes in Sodium-Ion Batteries. *J. Power Sources* **2016**, *320*, 49–58. [CrossRef]
105. Guo, X.; Wang, Z.; Deng, Z.; Li, X.; Wang, B.; Chen, X.; Ong, S.P. Water Contributes to Higher Energy Density and Cycling Stability of Prussian Blue Analogue Cathodes for Aqueous Sodium-Ion Batteries. *Chem. Mater.* **2019**, *31*, 5933–5942. [CrossRef]
106. Jeong, G.S.; Jung, K.H.; Choi, S.; Kim, K.C. Electrochemical Characteristics of Cyanoquinones as Organic Cathodes for High-Potential Sodium-Ion Batteries. *ACS Sustain. Chem. Eng.* **2020**, *8*, 11328–11336. [CrossRef]
107. Suriyakumar, S.; Mazumder, A.; Dilip, P.S.; Hariharan, M.; Shaijumon, M.M. Synergistically Improving the Stability and Operating Potential of Organic Cathodes for Sodium-Ion Battery. *Batter. Supercaps* **2023**, *6*, e202300111. [CrossRef]
108. Xie, B.; Zuo, P.; Wang, L.; Wang, J.; Huo, H.; He, M.; Shu, J.; Li, H.; Lou, S.; Yin, G. Achieving Long-Life Prussian Blue Analogue Cathode for Na-Ion Batteries Via Triple-Cation Lattice Substitution and Coordinated Water Capture. *Nano Energy* **2019**, *61*, 201–210. [CrossRef]
109. Sottmann, J.; Bernal, F.L.M.; Yusenko, K.V.; Herrmann, M.; Emerich, H.; Wragg, D.S.; Margadonna, S. In Operando Synchrotron Xrd/Xas Investigation of Sodium Insertion into the Prussian Blue Analogue Cathode Material $Na_{1.32}Mn[Fe(CN)_6]_{0.83} \cdot Z\ H_2O$. *Electrochim. Acta* **2016**, *200*, 305–313. [CrossRef]
110. Seok, J.; Yu, S.-H.; Abruña, H.D. Operando Synchrotron-Based X-Ray Study of Prussian Blue and Its Analogue as Cathode Materials for Sodium-Ion Batteries. *J. Phys. Chem. C* **2020**, *124*, 16332–16337. [CrossRef]

111. Wang, W.; Gang, Y.; Peng, J.; Hu, Z.; Yan, Z.; Lai, W.; Zhu, Y.; Appadoo, D.; Ye, M.; Cao, Y.; et al. Effect of Eliminating Water in Prussian Blue Cathode for Sodium-Ion Batteries. *Adv. Funct. Mater.* **2022**, *32*, 2111727. [CrossRef]
112. Xu, Y.; Wan, J.; Huang, L.; Ou, M.; Fan, C.; Wei, P.; Peng, J.; Liu, Y.; Qiu, Y.; Sun, X.; et al. Structure Distortion Induced Monoclinic Nickel Hexacyanoferrate as High-Performance Cathode for Na-Ion Batteries. *Adv. Energy Mater.* **2019**, *9*, 1803158. [CrossRef]
113. Peng, J.; Zhang, W.; Wang, J.; Li, L.; Lai, W.; Yang, Q.; Zhang, B.; Li, X.; Du, Y.; Liu, H.; et al. Processing Rusty Metals into Versatile Prussian Blue for Sustainable Energy Storage. *Adv. Energy Mater.* **2021**, *11*, 2102356. [CrossRef]
114. Nielsen, I.; Dzodan, D.; Ojwang, D.O.; Henry, P.F.; Ulander, A.; Ek, G.; Häggström, L.; Ericsson, T.; Boström, H.L.B.; Brant, W.R. Water Driven Phase Transitions in Prussian White Cathode Materials. *J. Phys. Energy* **2022**, *4*, 044012. [CrossRef]
115. Kuan, H.-C.; Luu, N.T.H.; Ivanov, A.S.; Chen, T.-H.; Popovs, I.; Lee, J.-C.; Kaveevivitchai, W. A Nitrogen- and Carbonyl-Rich Conjugated Small-Molecule Organic Cathode for High-Performance Sodium-Ion Batteries. *J. Mater. Chem. A* **2022**, *10*, 16249–16257. [CrossRef]
116. Shimizu, T.; Mameuda, T.; Toshima, H.; Akiyoshi, R.; Kamakura, Y.; Wakamatsu, K.; Tanaka, D.; Yoshikawa, H. Application of Porous Coordination Polymer Containing Aromatic Azo Linkers as Cathode-Active Materials in Sodium-Ion Batteries. *ACS Appl. Energy Mater.* **2022**, *5*, 5191–5198. [CrossRef]
117. Bridges, C.A.; Sun, X.-G.; Zhao, J.; Paranthaman, M.P.; Dai, S. In Situ Observation of Solid Electrolyte Interphase Formation in Ordered Mesoporous Hard Carbon by Small-Angle Neutron Scattering. *J. Phys. Chem. C* **2012**, *116*, 7701–7711. [CrossRef]
118. Sacci, R.L.; Bañuelos, J.L.; Veith, G.M.; Littrell, K.C.; Cheng, Y.Q.; Wildgruber, C.U.; Jones, L.L.; Ramirez-Cuesta, A.J.; Rother, G.; Dudney, N.J. Structure of Spontaneously Formed Solid-Electrolyte Interphase on Lithiated Graphite Determined Using Small-Angle Neutron Scattering. *J. Phys. Chem. C* **2015**, *119*, 9816–9823. [CrossRef]
119. Owejan, J.E.; Owejan, J.P.; DeCaluwe, S.C.; Dura, J.A. Solid Electrolyte Interphase in Li-Ion Batteries: Evolving Structures Measured in Situ by Neutron Reflectometry. *Chem. Mater.* **2012**, *24*, 2133–2140. [CrossRef]
120. Kawaura, H.; Harada, M.; Kondo, Y.; Kondo, H.; Suganuma, Y.; Takahashi, N.; Sugiyama, J.; Seno, Y.; Yamada, N.L. Operando Measurement of Solid Electrolyte Interphase Formation at Working Electrode of Li-Ion Battery by Time-Slicing Neutron Reflectometry. *ACS Appl. Mater. Interfaces* **2016**, *8*, 9540–9544. [CrossRef]
121. Simons, H.; King, A.; Ludwig, W.; Detlefs, C.; Pantleon, W.; Schmidt, S.; Stöhr, F.; Snigireva, I.; Snigirev, A.; Poulsen, H.F. Dark-Field X-Ray Microscopy for Multiscale Structural Characterization. *Nat. Commun.* **2015**, *6*, 6098. [CrossRef] [PubMed]
122. Sinha, S.K.; Jiang, Z.; Lurio, L.B. X-Ray Photon Correlation Spectroscopy Studies of Surfaces and Thin Films. *Adv. Mater.* **2014**, *26*, 7764–7785. [CrossRef] [PubMed]
123. Shpyrko, O. X-ray Photon Correlation Spectroscopy. *J. Synchrotron Radiat.* **2014**, *21*, 1057–1064. [CrossRef] [PubMed]

Disclaimer/Publisher's Note: The statements, opinions and data contained in all publications are solely those of the individual author(s) and contributor(s) and not of MDPI and/or the editor(s). MDPI and/or the editor(s) disclaim responsibility for any injury to people or property resulting from any ideas, methods, instructions or products referred to in the content.